J. Am. Ceram. Soc., 1–20 (2011)
DOI: 10.1111/j.1551-2916.2011.04599.x

journal

Protocols for the Optimal Design of Multi-Functional Cellular Structures: From Hypersonics to Micro-Architected Materials

Lorenzo Valdevit,[‡,†] Alan J. Jacobsen,[§] Julia R. Greer,[¶] and William B. Carter[§]

[‡] Mechanical and Aerospace Engineering Department and Chemical Engineering and Materials Science Department, University of California, Irvine, California, 92697

[§] HRL Laboratories, Malibu, California, 90265

[¶] Materials Science Department, California Institute of Technology, Pasadena, California, 91125

Cellular materials with periodic architectures have been extensively investigated over the past decade for their potential to provide multifunctional solutions for a variety of applications, including lightweight thermo-structural panels, blast resistant structures, and high-authority morphing components. Stiffer and stronger than stochastic foams, *periodic* cellular materials lend themselves well to geometry optimization, enabling a high degree of tailorability and superior performance benefits. This article reviews a commonly established optimal design protocol, extensively adopted at the macro-scale for both single and multifunctional structures. Two prototypical examples are discussed: the design of strong and lightweight sandwich beams subject to mechanical loads and the combined material/geometry optimization of actively cooled combustors for hypersonic vehicles. With this body of literature in mind, we present a motivation for the development of *micro-architected materials*, namely periodic multiscale cellular materials with overall macroscopic dimensions yet with features (such as the unit cell or subunit cell constituents) at the micro- or nano-scale. We review a suite of viable manufacturing approaches and discuss the need for advanced experimental tools, numerical models, and optimization strategies. In analyzing challenges and opportunities, we conclude that the technology is approaching maturity for the development of micro-architected materials with unprecedented combinations of properties (e.g., specific stiffness and strength), with tremendous potential impact on a number of fields.

I. Introduction

Stochastic cellular materials (i.e., foamed materials that contain significant amounts of porosity) have long been used for their low weight, high sound absorption, crashworthiness, and thermal properties.[1] Approximately 15 years ago, advances in manufacturing technologies spearheaded a large academic and industrial interest in metallic foams,[2] which combine all the properties listed above with increased specific strength and stiffness and high-temperature capabilities. An important feature of open-cell foams is the interconnected open space, which can be employed to enable additional capabilities, such as active cooling[2,3] or energy storage,[2,4–6] thus enabling multifunctionality. More recently, detailed mechanical experiments on metallic foam-based sandwich panels under bending and compressive loads revealed that all foams are bending-dominated, i.e., they deform by compliant and weak bending modes of the cell walls and ligaments, inefficiently using the base constituent material in the foam by leaving much of it out of the load path.[7–9] In addition, their stochastic nature inevitably introduces imperfections that further depress their mechanical properties.[10] Vastly increased specific stiffness and strength (i.e., stiffness and strength per unit weight) can be obtained in *periodic cellular architectures* (such as those depicted in Fig. 1); if designed properly, under global bending and compressive loadings these architectures will deform by stretching of the ligaments, a stiff and strong local deformation mode that makes maximal use of the base constituent and maximizes load carrying capacity.[4,11] As an additional benefit over "semi-engineered" open-cell foams, periodic cellular topologies have many more geometrical features that can be engineered and optimized. A large body of research has been published in the past decade on optimally designed metallic periodic cellular systems, with emphasis on specific strength,[11–17] active cooling,[18] and combinations thereof,[19–21] combined strength and thermal conductivity (through a heat pipe design),[22] high-velocity impact absorption,[23–26] and high-authority shape morphing potential.[27–31]

In spite of the variety of applications (each imposing different objective functions and constraints), the same protocol for optimal design has been consistently (and successfully) adopted in nearly all cases. This protocol consists of a combination of analytical, numerical, and experimental techniques, and is reviewed in Section II of this article, with emphasis to mechanical and thermo-mechanical optimization. In Section III of this article, we pose three questions: (i) Are there any mechanical benefits in designing *micro-architected materials* (namely, macro-scale periodic cellular materials with unit cells at the micro-scale)? (ii) Are there suitable and cost-effective manufacturing processes for micro-architected materials? (iii) Is the optimal design protocol (including analytical, numerical and experimental techniques) which has been successfully adopted for large-scale structures appropriate to harness the full potential of micro-architected materials? By answering these questions, we conclude that the technology is approaching maturity for the development, characterization, and optimal design of a novel class of multifunctional materials with the potential to achieve unprecedented combination of properties.

II. Micro-Architected Materials

This section briefly reviews the well-established optimal design protocol for cellular periodic structures. Manufacturing approaches are described first, to offer a flavor of the topologies and materials combination that are readily available. The optimal design protocol (consisting of a combination of

T. M. Pollock—contributing editor

Manuscript No. 28794. Received October 16, 2010; approved April 02, 2011.
[†]Author to whom correspondence should be addressed. e-mail: valdevit@uci.edu

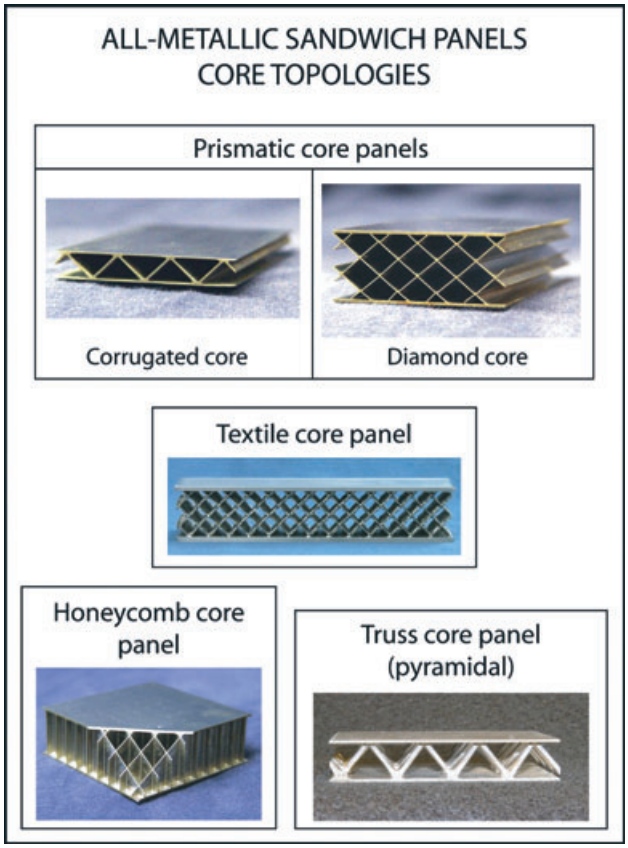

Fig. 1. Examples of all-metallic sandwich panels manufactured by Transient Liquid Phase (TLP) bonding. Modified from Lu *et al.*[3]

analytical, numerical, and experimental techniques) is presented for two archetypal structures: a simple single-function structure (a lightweight periodic sandwich beam with a prismatic corrugated core, designed for resistance to mechanical loads—bending and transverse shear), and a more complex multifunctional structure (a lightweight actively cooled sandwich plate, designed for resistance to mechanical and thermal loads—and additional design constraints). The latter is presented in the context of materials development for hypersonic vehicles. In both cases, materials selection is addressed.

(1) Manufacturing Approaches

Reliable manufacturing techniques have been developed for metallic sandwich structures with a number of core topologies. Cores are generally assembled by folding a plate (as in case of corrugated cores or truss cores) or slotting and assembling a large number of beam and/or plate elements (honeycomb cores, diamond prismatic cores, textile cores); in the latter case, the constituents need to be metallurgically bonded to impart strength and stiffness to the structure.[6] In both approaches, face sheets are bonded to the core. As bonded nodes are inevitably subjected to substantial in-service loads (in tension, compression and shear), a manufacturing process that results in strong nodes is essential. For a number of materials such as steels, copper, and aluminum alloys, Transient Liquid Phase Bonding (TLP), a high-temperature brazing process involving significant inter-diffusion at the joints, is the ideal technique.[32] TLP enables much stronger structures than conventional, lower-temperature brazing because the resulting nodes have nearly the same chemical composition as the base metal. TLP is also better than welding, both for simplicity and scalability (all the nodes are formed at once, without need for line-of-sight access) and because solidification at the brazing temperature ensures much lower residual stresses in the bonded region compared to welding. Examples of sandwich panels with various core topologies obtained with TLP are provided in Fig. 1. Most of the experimental work published to date on all metallic sandwich panels pertains to steel panels, for which TLP brazing agents are readily available. TLP recipes for aluminum and copper alloys also exist.[33]

Recently, alternative manufacturing approaches were developed for aerospace-relevant high-temperature alloys. Titanium (Ti6Al4V) panels were manufactured with diffusion bonding, resulting in good nodal microstructure and strengths.[34] The extension to even higher temperatures requires nickel superalloys. Unfortunately, high-strength, γ'-rich nickel superalloys are not formable at room temperature. A clever solution for thin-gage panels was recently proposed, whereby a formable, single-phase γ-Ni superalloy is assembled in the right shape, all the components are assembled via TLP bonding, and subsequently the finished structure is aluminized and precipitation hardened, resulting in a high-strength, γ'-rich alloy.[35]

For lower temperature applications, polymer-matrix composites (e.g., Carbon-epoxy) are available with significantly higher weight efficiency than other metals.[36] The primary manufacturing issue is ensuring sufficient nodal strength. Carbon-epoxy honeycomb core panels obtained by a slotting procedure were recently demonstrated and optimized for compressive loads.[37] For corrugated core panels, 3D weaving is a natural option, albeit at an increase in cost and manufacturing complexity.[38] A number of simpler, prepreg-based approaches are currently under consideration.[36]

(2) Design Protocol for Maximum Specific Strength

Periodic cellular materials have the prominent feature of being naturally suitable to optimization. In addition to selecting the ideal base material (or combinations thereof in the case of a hybrid), the architecture can be optimized for a specific objective (or multiple objectives) subject to a number of constraints. The general multi-step procedure can be summarized as follows:

1. Fundamental properties of the base material(s) are obtained, either from data sheets or through appropriate experimental characterization, e.g., dog-bone tensile testing resulting in a stress-strain curve—possibly including temperature and time effects: visco-elasticity, visco-plasticity, fatigue, etc.
2. The evolution of the variables of interest (stress, strain, temperature, electric potential, etc.) is modeled analytically as a function of the structure geometry and the applied loads (mechanical, thermal, electrical, etc.). Constraints are formulated for the specific application under consideration (e.g., no yielding or buckling anywhere in the structure, no melting of the material).
3. Numerical analyses are performed, typically employing commercial Finite Elements packages, to verify the validity of the simplifying assumptions underlying step (2).
4. A combination of steps (2) and (3) is coupled with an optimization routine (quadratic optimizers for convex problems, discrete algorithms for problems featuring many local minima) and the structure geometry and/or material are optimized subject to all the prescribed constraints. The objective function strongly depends on the specific problem.
5. A prototype (possibly to scale) of the *entire* optimal or near-optimal structure (or at least substructure) is manufactured and its performance is verified *experimentally* to verify all the modeling assumptions (underlying both (2) and (3)).

As an example, we examine optimization of a metallic corrugated-core sandwich panel loaded by any combination of bending and transverse shear loads (Fig. 2(a)).[12,13] The objec-

tive is maximum strength at a prescribed weight. Nondimensional load intensity and weight are defined as:

$$\Pi = \frac{V^2}{EM}$$
$$\psi = \frac{W}{\rho \ell^2} = 2\frac{d_f}{\ell} + \frac{1}{\cos\theta}\frac{d_c}{\ell} \quad (1)$$

where V and M are the maximum shear force and bending moment per unit width of the panel, respectively, $\ell = M/V$ is the governing length-scale in the problem, E and ρ are the Young's modulus and density of the base material, respectively, and the geometric variables d_f, d_c, θ are defined in Fig. 2(a). The length-scale ℓ defines the actual loading condition (e.g., $\ell = L/2$ for three-point bending, L being the span of the panel between the loading points); normalizing all the dimensions with ℓ renders generality. Four possible failure mechanisms are identified: face (FY) and core (CY) yielding, and face (FB) and core (CB) buckling. For transverse loadings (bending about an axis parallel to the corrugation—Fig. 2(a)), analytical expressions are readily derived:

$$\left(\frac{V^2}{EM}\right)_{FY} = \frac{\varepsilon_Y d_f}{\ell}\left(\frac{H_c}{\ell} + \frac{d_f}{\ell}\right)$$
$$\left(\frac{V^2}{EM}\right)_{CY} = \frac{\varepsilon_Y d_c \sin\theta}{\ell}$$
$$\left(\frac{V^2}{EM}\right)_{FB} = \frac{k_f \pi^2 \tan^2\theta}{48}\left(\frac{H_c}{\ell} + \frac{d_f}{\ell}\right)^{-1}\left(\frac{d_f}{\ell}\right)^3 \quad (2)$$
$$\left(\frac{V^2}{EM}\right)_{CB} = \frac{k_c \pi^2 \sin^3\theta}{12}\left(\frac{H_c}{\ell} + \frac{d_f}{\ell}\right)^{-2}\left(\frac{d_c}{\ell}\right)^3$$

where ε_Y is the yield strain of the constituent material. Similar equations can be derived for longitudinal loadings. Note that ε_Y is the *only* material property governing the problem. The implication is that the optimal material for a corrugated-core sandwich panel subject to any combination of bending and transverse shear loads is simply the material with the largest yield strain. The same conclusion applies to any other core topology and a number of mechanical loading conditions. This important result allows separation of materials selection and optimal topological design. Multifunctional problems involving more complex physics often lack this feature, requiring material and topology to be concurrently optimized (see Section II(3)).

The interplay of failure mechanisms is best illustrated with failure mechanisms maps (Fig. 2(b)). If the corrugation angle, θ, and the panel weight, Ψ, are fixed, panel geometry is entirely defined by the thickness of the core, H_c and face sheet, d_f. Hence, each point on the map represents a possible panel design, with all designs having the same weight. The various regions denote design spaces where panel strength is governed by each failure mechanism (core yielding is never active under these loading conditions and weight). Strength contours (expressed in nondimensional form) clearly identify that the best design occurs at the intersection of three failure mechanisms (Incidentally, the confluence of three failure mechanisms at the optimal design point is a recurring feature for many core topologies,[11,12,15–17,39] but this condition is not universal (C. A. Steeves, Personal Communication).

Before it can be used with confidence, this model needs to be verified with a combination of numerical (FE) analyses and validated with a selected set of experiments. Figure 2(c) shows excellent agreement between analytical (white dot) and numerical predictions with experimental results for one particular design loaded in three-point bending (black dot in Fig. 2(b)). The inset in Fig. 2(c) compares the deformed shape of the panel at the end of the experiment. Note that both face and core buckling are evident (face yielding was also verified with a strain gage during the experiment), consistent with the analytical predictions of Fig. 2(b).

Numerical and experimental validation of the analytical model allows computationally efficient design optimization for a wide range of applied load intensities. With reference to Eqs. (1–2), the problem can be stated as follows: for any given load intensity, Π, minimize the panel weight, Ψ, subject to four constraints ($\Pi < \Pi_{FY}$, $\Pi < \Pi_{FB}$, $\Pi < \Pi_{CY}$, $\Pi < \Pi_{CB}$). As all functions are convex, a simple quadratic optimizer was successfully used. Results for aluminum panels are presented in Fig. 2(d). This master figure compares the weight efficiency of a number of optimally designed core topologies; the corrugated core panel loaded transversely (discussed herein) is much lighter than solid plates, but more efficient topologies can be devised (hexagonal honeycombs are optimally efficient in this loading condition, and have often been used as benchmarks).

(3) Design Protocol for Multifunctional Structures: An Example From Hypersonics

(A) Preliminaries: For multifunctional applications, the challenge is choosing a cellular material with the best combination of constituent material and architecture to optimize all the desired objective functions under a series of design constraints. The multi-step protocol of Section II(2) can be adapted to this more challenging scenario, although the computational intensity quickly grows as the physics of the problem becomes more complex. Herein, we discuss the optimization of a simple architected material (a prismatic sandwich panel with hollow rectangular channels) for minimum weight under the simultaneous application of mechanical and thermal loads (subject to a number of design constraints). The motivation is a feasibility study for metallic actively cooled combustors for hypersonic vehicles (Fig. 3(a)). Details beyond this concise treatment are provided in a number of references.[19–21,40]

(B) Thermo-Mechanical Loads on Combustor Wall of a Hypersonic Vehicle: Whereas acreage (and to some extent, leading edges) of thermally balanced hypersonic vehicles can be engineered to passively dissipate heat by radiation, combustor walls inevitably require active cooling strategies to contend with the large heat fluxes arising from the combustion process. The prototypical structure, a sandwich panel with prismatic channels that provide active cooling by the fuel before injection (Fig. 3(b)), is subjected to significant thermo-mechanical loads. The thermal loads are represented by a heat transfer coefficient and a hot gas temperature on one side of the panel. The mechanical loads are (i) pressure in the combustion chamber (which, depending on the boundary conditions, can induce panel-level bending), and (ii) pressure in the cooling channels (dictated by fuel injection requirements). As a result, significant thermo-mechanical stresses arise. Withstanding these stresses at operating temperatures necessitates careful design. A viable solution must resist several failure modes: yielding or rupture due to (a) thermal stresses, (b) pressure or inertial stresses, (c) combined thermo-mechanical stresses, as well as (d) softening of the material, (e) coking of the coolant, and (f) excessive pressure drop in the cooling ducts. The objective is twofold: (i) identify the optimal material and (ii) optimize the structure for minimum weight. The challenge is to assure that none of the failure modes is active over the pertinent ranges of coolant flow rate, V_{eff} (often nondimensionally expressed in terms of the air/fuel mixture richness, ϕ, relative to stoichiometric combustion) and thermal loads (expressed by the heat-transfer coefficient between the combustion gas and the solid surface, h_G). The intensity of the mechanical loads is assumed constant for simplicity. Geometry and loads are depicted in Fig. 3(b).

(C) Optimal Design Protocol: The multi-step approach of Section II(2) is applicable, albeit with the complication that even a simplistic analytical model precludes the extraction of a

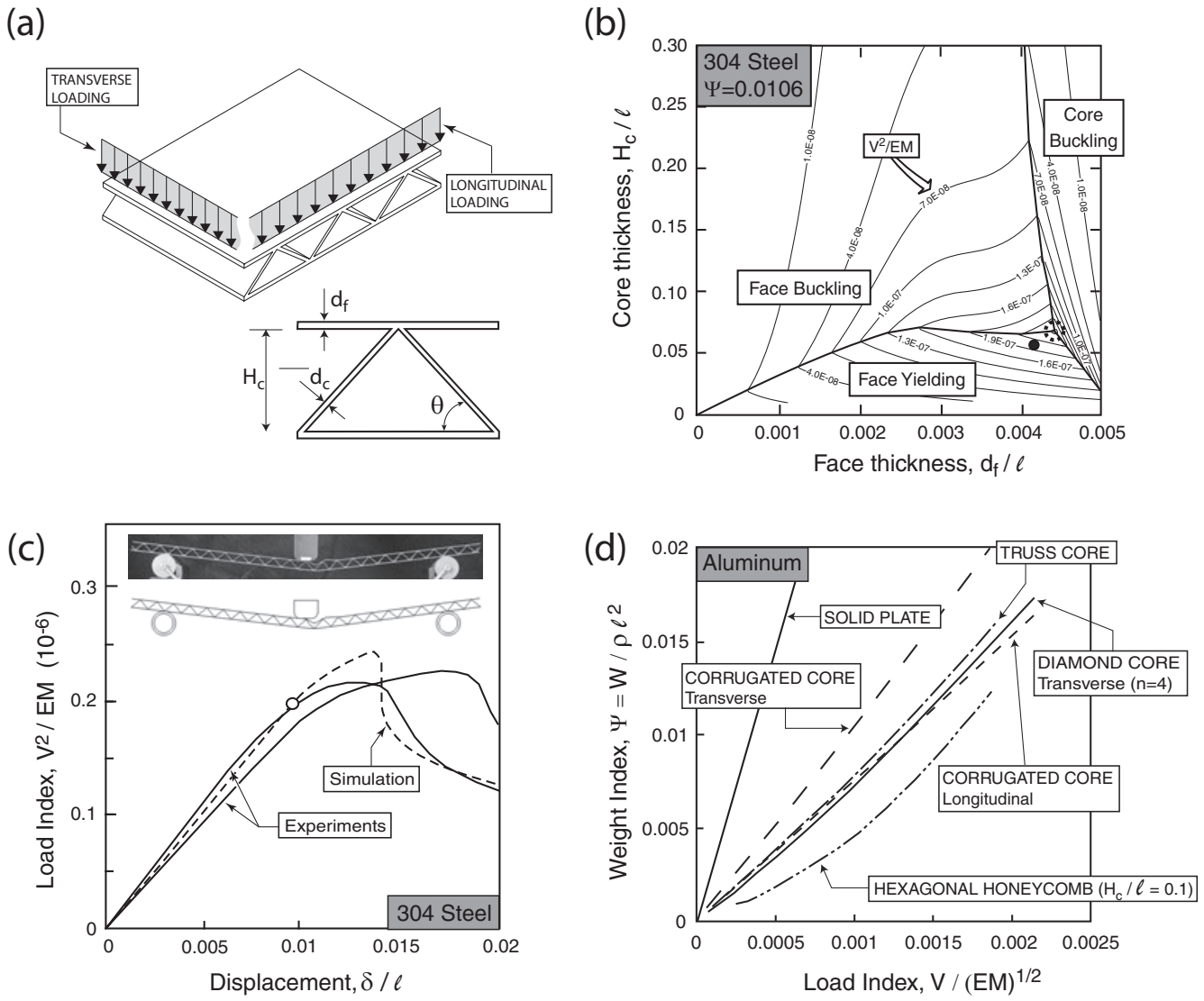

Fig. 2. (a) Schematic of a corrugated-core sandwich panel loaded with a combination of moment and transverse shear. Two loading directions (referred to as transverse and longitudinal) are indicated. (b) Failure map for steel corrugated core panels loaded in the transverse direction. Each point represents a different design (all at the same weight). In this case, the confluence of the three regions denotes the maximum strength design. (c) Comparison of analytical and numerical predictions and experimental results for a 3-point bending experiment on the steel corrugated core panel indicated by a black dot in (b). (d) Weight-efficiency of optimized aluminum panels for a number of core topologies. Adapted from Valdevit *et al.*[12,13]

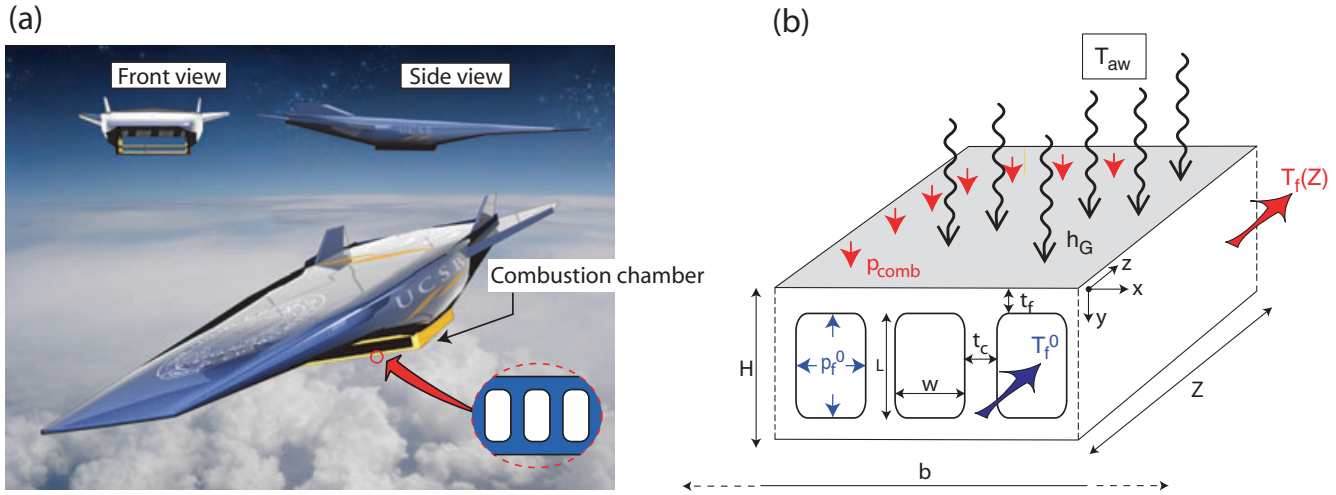

Fig. 3. (a) Schematic of an air-breathing hypersonic vehicle. (b) Archetypal actively cooled combustor with applied loads.

simple materials performance index. The implication is that materials and structural designs must be tackled concurrently. A flowchart of the optimization protocol is presented in Fig. 4. To explore the feasibility of a number of materials over a series of operating conditions, ranges of thermal load (i.e., heat transfer coefficient from the combustor side), and cooling efficiency (i.e., coolant flow rate) are explored. A suite of high-temperature metallic materials were investigated (with and without thermal barrier coatings[19]), all benchmarked with the state-of-the-art ceramic matrix composite C-SiC. Integration of the actively cooled panel with the rest of the vehicle largely affects the thermo-mechanical stresses. Although several conditions were investigated, herein we will focus on a flat panel supported in discrete locations, separated by a span, L. Once a material is chosen, and specific values of thermal loads and cooling efficiency are selected, the thermo-mechanical problem is fully defined. Analytical models based on a thermal network and plate/beam theory provide the temperature and stress distributions. Please see Valdevit *et al.*[19] for details. The accuracy of these models was checked against selected Computational Fluid Dynamics (CFD) and Finite Elements calculations. The model/FE agreement for the Von Mises stress distribution is illustrated in Fig. 5. The graphs track stress variations along four paths in the unit cell. Notice that the agreement for thermal, mechanical, and thermo-mechanical stresses is excellent throughout, except for two cases. (a) At the internal nodes (points 2 and 3 in Fig. 5), significant stress intensifications (naturally not predicted by the analytical model) arise. This discrepancy is disregarded for three reasons[19]: (i) For this particular simulation, the temperatures at the corners are relatively low (and hence the yield strength relatively high), so that the corners remain elastic. We speculate that this concept generalizes to all metallic systems of interest, although a formal proof requires further analysis. (ii) The fillet radius can be increased in actual designs, ameliorating the stress intensification. (iii) Local plasticity at the nodes upon a few cycles can be accepted, provided that it is followed by shakedown. (b) Thermal stresses are underpredicted by ~20% at the cold face (points 3, 4, 7, and 8 in Fig. 5). This discrepancy can be related to modeling assumptions. Simple expressions for the thermal stresses were obtained assuming that the entire core is at the same temperature as the cold face sheet. FE analyses confirmed that this assumption results in accurate stress predictions on the hot face, whereas it underestimates the thermal stress in the cold face. As the yield strength of the materials decreases with increasing temperature, the cold face is never prone to failure, rendering this inaccuracy inconsequential.

Once the analytical model is validated by numerical analyses, it can be successfully used for efficient optimization studies (Experimental investigation is ultimately necessary to close the design loop, but this requires substantial dedicated test facilities and is beyond the scope of this work). A simple quadratic optimizer (FMINCON, available in the MATLAB suite) is used to minimize the panel mass subject to the constraints defined above. As this thermo-mechanical problem is more complex than the simple mechanical optimization discussed in Section II(2) (in that a number of local optima arise), a set of randomly generated initial guesses is introduced to seek the global optimum. An alternative would be the use of discrete (i.e., non gradient-based) optimization algorithms, inherently more robust against local optima (see Section III(5)(C)). When the optimizer finds a solution, the set of geometric parameters yielding the minimum weight design is stored. Conversely, when the optimizer fails to find a solution within the standard number of iterations defined in FMINCON, the material under consideration is deemed unfeasible for the specific set of thermal loads and cooling efficiency. The procedure is repeated for a set of points scanning the thermal loads/cooling efficiency space, and for a suite of high-temperature materials.

(D) Results: Optimal Designs and Ideal Materials: The ensuing information can be presented in two complementary ways: (i) materials robustness maps (Fig. 6(a)) and (ii) weight-efficiency plots (Fig. 7). Materials robustness maps depict the region in the thermal load/cooling efficiency space where a given material provides a feasible solution, irrespective of its weight (orange area in the maps of Fig. 6(a)). The gray area in the maps extends the feasible region to higher thermal loads and/or lower cooling efficiency by allowing a thermal barrier coating to be interposed between the panel hot side and the combustion chamber (A conventional YSZ columnar TBC is assumed, with through-thickness thermal conductivity of 1 W/m K, in-plane conductivity of 0 W/m K, and mass density of 3000 kg/m^3). The TBC thickness (not to exceed 300 μm and 25% of the face sheet thickness) is chosen by the optimizer, as a compromise between added weight and reduced temperatures in the underlying metallic structure (See Valdevit *et al.*[19] and Vermaak *et al.*[21] for details). Four different materials are illustrated in Fig. 6(a): a Niobium alloy (C-103), the ceramic matrix composite C-SiC (benchmark material), a high-temperature Copper alloy (GrCop-84), and a Nickel superalloy (Inconel X-750). Materials properties are provided in Valdevit *et al.*[19] and Vermaak *et al.*[21] For the particular set of boundary conditions adopted here, the four materials show similar robustness (loosely defined as the area of design feasibility), but this conclusion can change greatly as the span between panel supports is shortened.[19,21]

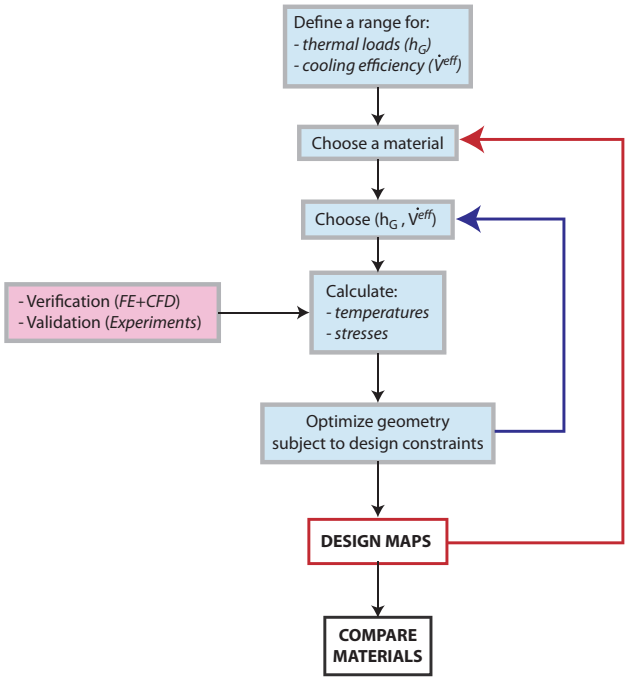

Fig. 4. Optimal design protocol for the combined geometry/materials selection of actively cooled panels for combustor liners in hypersonic vehicles. Reprinted from Valdevit *et al.*[19]

Importantly, the optimal design tool described in Section II(3)(C) (and depicted schematically in Fig. 4) can be used as a preliminary screening tool for new materials development. The mechanical properties of Inconel X-750 can be improved by alloying or heat treatment, generally resulting in increased flow stress or increased softening temperature, but not both in the same material (Fig. 6(b)). The question is which of the two property improvements would be most beneficial to the application being considered. The answer is provided in Fig. 6(c); for the boundary conditions used in this study, a 20% increase in the flow stress (without extending the softening temperature) has a much larger impact on the robustness of the material than a similar increase in softening temperature (without elevating the flow stress). Again, the conclusion changes if the panel span is shortened. This information is very important for the materials developer, and it

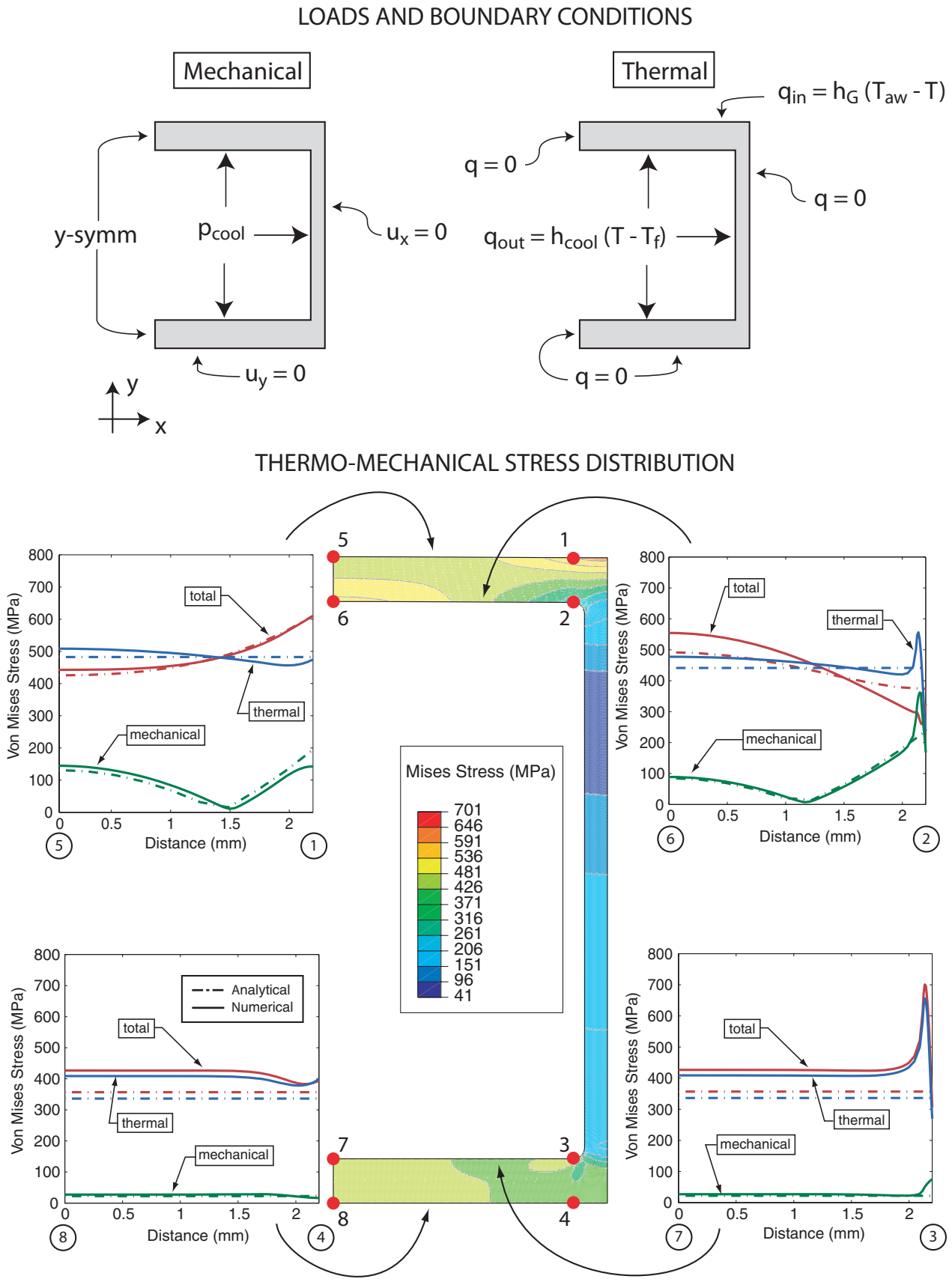

Fig. 5. Comparison of analytical and numerical (FE) von Mises stress distributions for an optimal actively cooled Inconel X-750 panel. The insets show the results for thermal, mechanical, and combined thermomechanical stresses along the four paths depicted. With the exception of Points 2 and 3, clearly affected by stress intensification, the agreement is very satisfactory, validating the optimization results presented in Fig. 6. Modified from Valdevit *et al.*[19]

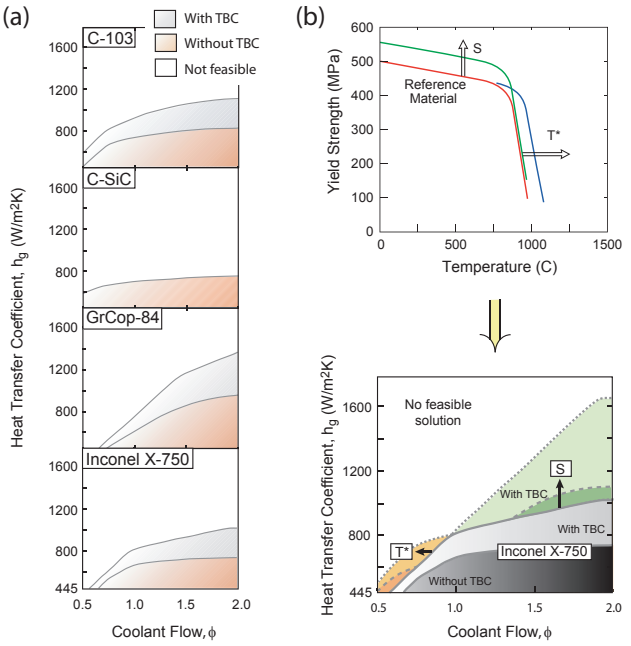

Fig. 6. (a) Performance maps for a number of candidate high-temperature materials for actively cooled walls of hypersonic combustors. The normalizing parameter for the coolant flow equivalence ratio ($\phi = f/f_{st}$) is that expected for steady-state Mach 7 flight conditions. Each map is the result of two independent optimizations. One (yellow) is performed absent a coating. When solutions exist only with a coating (light gray), the optimization is conducted using the TBC thickness as a variable. Areas without a feasible solution are in white. (b) Reclaimed feasibility space provided by two notional materials based on INCONEL X-750. The first notional material (designated S), examines the effect of elevating the yield strength at intermediate temperatures by 25%, whereas the second (designated T*) probes the effect of extending the maximum use temperature by 25%; analyses are shown both with (light) and without (dark) a TBC. For comparison, the notional results are superimposed on the original performance maps for INCONEL X-750 (Modified from Vermaak *et al.*[21])

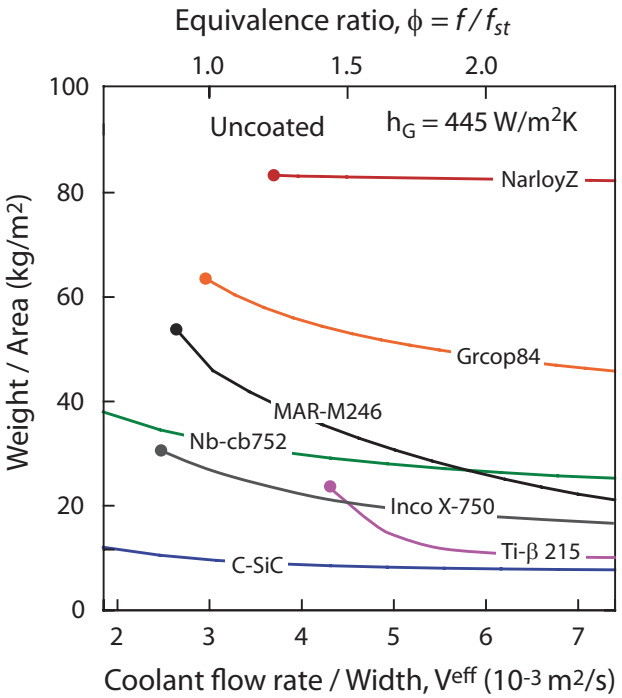

Fig. 7. Weight efficiency of different material candidates for actively cooled walls of hypersonic combustors. The equivalence ratio, ϕ, is defined as for Fig. 6. From Valdevit *et al.*[19]

is not readily accessible in any other forms (i.e., it does not transparently appear from the equations for temperature and stress distributions). This is a perfect example of the need for efficient optimal design tools to tackle these inherently multi-functional problems.

In Fig. 7, we show weight efficiency for a specific thermal load (realistic for a Mach 7 hydrocarbon-powered vehicle). Each curve tracks the minimum weight of an optimized structure for a given material. Notice that different materials have vastly different weight efficiencies, even if their robustness (the area of the curve in Fig. 6(a)) is somewhat similar. The benchmark material, C-SiC, offer by far the lowest weight. High-temperature titanium alloys (Ti-β 215) offer the lightest metallic systems, but their feasibility is limited to low thermal loads. Among the metals that offer robust solutions over a range of thermal loads, Niobium alloys (e.g., Nb-cb752, C-103) and Nickel superalloys (e.g., Inconel X-750, MAR-M246) are the most promising materials. Allowing the metals to shakedown upon thermo-mechanical cycling results in lighter systems (by as much as 30%–40%, depending on the boundary conditions), further increasing the competitiveness of metallic solutions.[40]

In closing, notice that all these conclusions are not transparently available from the equations, as thermal and mechanical properties are deeply intertwined in this heavily constrained thermo-mechanical problem.

III. Optimal Design of Micro-Architected Cellular Materials

In this section, we present the case for the development of a new class of multifunctional materials, characterized by a periodic cellular architecture with unit cell at the micro-scale and a characteristic dimension for the constituent material in the sub-micrometer region. If manufactured and designed correctly, *these micro-architected materials enable exploitation of potentially useful nano-scale mechanical effects (e.g., size effects in plasticity and fracture) that enhance mechanical properties relative to bulk macro-scale structures*. After reviewing viable manufacturing schemes to exploit this vision, we present the technical rationale for the expected performance and assess both the applicability of the multi-step optimal design approach described in Section II and the availability of suitable experimental and computational tools. In the interest of brevity we focus on mechanical design, although similar concepts can be extended to other functionalities.

(1) Manufacturing Approaches

A viable manufacturing approach for lattice-based micro-architected materials must possess the following key features: (i) dimensional control down to the 0.1–10 μm range; (ii) scalability to macroscopic part dimensions; and (iii) acceptable throughput to enable cost-effective manufacturing. Architectural flexibility (i.e., the capability to generate different unit cell topologies) and a wide suite of base materials are additional desirable attributes. To the best of the authors' knowledge, three families of manufacturing approaches exist today for the fabrication of lattice-based micro-architected materials: scaled-down versions of wire layup[41] and other modular assembly methods[42] (discussed in Section II(1)), stereolithography[43] (including the most advanced 2-photon approach[44]), and a new self-propagating photopolymer waveguide (SPPW) process,[45] recently developed at HRL Laboratories. Key attributes of each method are assessed in Table 1. Modular assembly methods can be useful for a wide range of end-materials, but are currently limited by the achievable resolution (minimum unit cell sizes ~100 μm and minimum feature

sizes ~10 μm) and scalability (as the number of unit cells becomes very large, the assembly procedure becomes more and more cumbersome). Stereolithography allows incredible resolution (sub-micron feature sizes and unit cells of the order of a few microns for the most recent two-photon process) and nearly infinite architectural freedom (virtually anything that can be CAD drawn can be made). As a serial process, stereolithography is extremely slow: for a given sample size, the total processing time roughly scales with the inverse of the minimum feature size, implying that macroscopic quantities of micro-architected materials could take days to make. For proof-of-concept and basic research, stereolithography is a very powerful technique, but its difficult scalability makes it currently inadequate for industrial processing.

For a wide range of desirable end-geometries, the best compromise among resolution, architectural freedom, and scalability may be provided by the SPPW process.[45] Polymeric lattices are formed by UV exposure of a two-dimensional photolithographic mask with a pattern of circular apertures that is covering a reservoir containing an appropriate photomonomer (Fig. 8). Within the photomonomer, self-propagating polymer waveguides originate at each aperture in the direction of each collimated UV beam, forming a three-dimensional array of polymer fibers that polymerize together at all points of intersection. After removing the uncured monomer, three-dimensional lattice-based open-cell polymeric materials can be rapidly fabricated. Although this method does not allow for *arbitrary* shapes to be formed within the starting resin bath, it has the potential to form a wide range of free-standing 3D polymer structures based on linear mechanically efficient truss-type elements. In striking contrast with stereolithography, the optical waveguide process can form all truss-type elements in the structure in parallel with a single exposure step, typically lasting less than 1 min. With current UV exposure capabilities, cellular materials with truss member diameters ranging from ~10 μm to >1 mm and a relative density <5% up to 30% have been demonstrated.[46] The overall material thickness, H, can range from 100 μm to over 25 mm (although generally $H < 100 \cdot d$, where d is the truss diameter). Examples of ordered unit cell architectures with different symmetries are shown in Fig. 9; however, this process is not limited to such architectures. Nonsymmetric architectures, functionally graded materials, and hierarchical micro-lattice structures are all easily obtained.

For manufacturing techniques that result in a polymer template, such as stereolithography and the SPPW process, a number of postprocessing techniques are available to replicate the micro-architectural features with a metal or a ceramic[47,48] (Fig. 10). Continuous metallic film, such as nickel, can be deposited by electroplating or electroless process on the surface of the polymer micro-lattice structure and the polymer template can be subsequently removed with a chemical etch.[49] Controlled thickness coatings are obtained by varying the plating time. Ceramic films can be deposited with chemical vapor deposition (CVD) techniques. To withstand the high temperatures required for CVD of refractory metals or ceramics, the polymeric template must be pyrolyzed with minimal geometric distortion as recently demonstrated.[50] After the CVD process, the carbon micro-lattice template can be removed by oxidation (>600°C in air), leaving a hollow tube ceramic micro-lattice structure, such as the SiC sample shown in Fig. 10.

One key advantage of the polymer→metal or polymer→ceramic conversion process is to capture the strengthening effects associated with a constituent material in thin-film form factor in a bulk form (Section III(2)). These "film form" properties generally require film thicknesses in the micro- (or even nano-) scale, dictating truss diameters ~10–100 μm. This makes the fabrication approach described above ideally suited for fabricating optimal open-cell periodic architectures with exceptionally strong metallic or ceramic constituent materials.

(2) Challenges and Opportunities

The lattice materials manufactured with the SPPW process described in Section III(1) possess two distinct features, not readily available with competing concepts: (i) *hollow truss configurations* and (ii) *multi-scale architectures*, with global sample size on the order of several inches and sub-millimeter unit cell dimensions. These two features provide unique opportunities to expand the current bounds of material properties spaces and achieve combinations of properties currently unavailable in any existing material (including the macro-scale architected materials described in Section II). The target regions for specific strength and stiffness are depicted in Fig. 11. Importantly, micro-architected materials fabricated as described herein maintain an open core architecture, enabling multifunctionality: with reference to Section II(3), strong and stiff structures amenable to efficient active cooling are obviously an attractive possibility. Herein, we briefly review the rationale for these opportunities (limiting our attention to mechanical properties), and summarize the outstanding challenges that must be overcome in order to exploit the full potential of micro-architected materials.

(A) Advantages of a Hollow Truss Configuration: Under any mechanical loadings, the strength of metallic lattice materials designed to operate in the elastic regime is limited by the onset of either yielding or elastic buckling. A simple analysis reveals the benefits of a hollow truss configuration; uniform compressive loading is assumed for simplicity, but the same conclusions qualitatively apply to other loading conditions. Consider a lattice material with a solid truss pyramidal unit cell, defined by truss member length, l, truss diameter, $2a$, and truss angle, ω. The relative density can be expressed as[51]:

$$\bar{\rho} = \frac{2\pi}{\cos^2\omega \sin\omega}\left(\frac{a}{l}\right)^2 \tag{3}$$

and the compressive strength is:

$$\frac{\sigma_{\text{comp}}}{\sigma_{\text{bar}}} = \bar{\rho}\sin^2\omega \tag{4}$$

where $\sigma_{bar} = \min\{\sigma_Y, \sigma_b\}$ represents the strength of the individual truss member, with σ_Y the yield strength of the base material and $\sigma_b = k^2\pi^2 E a^2/4l^2$ the elastic buckling strength. For conservativeness, it is customary to idealize each bar as pin-jointed, resulting in $k = 1$. Solid truss lattice materials are buckling-limited at low relative density, and transition to the yielding-limited regime at $\bar{\rho}_{trans} = 8\varepsilon_Y/(\pi \sin\omega\cos^2\omega)$ (Fig. 12). For most metals, assuming a truss angle of 45–70°, the yield strain $\varepsilon_Y \sim 10^{-3}$, indicating a transition at $\bar{\rho} \sim 1 - 2\%$. As trusses with relative densities <<1% can be manufactured with the approach described in Section III(1), the implication is that the lightest lattice materials based on solid trusses will be inevitably buckling-dominated. The situation improves when hollow trusses are employed. Invoking a thin-wall approximation, the relative density of hollow truss structures scales as:

$$\bar{\rho} = \frac{4\pi}{\cos^2\omega \sin\omega}\left(\frac{a}{l}\right)\left(\frac{t}{l}\right) \tag{5}$$

with t the truss wall thickness. The compressive strength scales as before, but the strength of the bar, σ_{bar}, is now:

$$\sigma_{\text{bar}} = \min\begin{cases} \sigma_Y & \text{yielding} \\ \sigma_{\text{gb}} = \dfrac{k^2\pi^2 E a^2}{2l^2} & \text{global (Euler) buckling} \\ \sigma_{\text{lb}} = \dfrac{E}{\sqrt{3(1-\nu^2)}}\dfrac{t}{a} & \text{local buckling} \end{cases} \tag{6}$$

The local buckling load corresponds to the chessboard mode.[52] Again, we assume $k = 1$ in the global buckling

Table 1. Comparison of Known Fabrication Methods for Open-Cellular Lattice-Type Materials. Reported Values Have Been Extrapolated Based on Published Techniques. Modified From Jacobsen *et al.*[46]

Approach to lattice-type cellular structures	Wire or textile layup; modular assembly[41,42]	Stereolithography[43]	2-photon stereo-lithography[44]	Self-propagating polymer waveguide (SPPW) process[45]
Unit cell type	3D Periodic	3D Periodic or aperiodic	3D Periodic or aperiodic	3D, Periodic or aperiodic
Multiple sizes of trusses in unit cell	Difficult	Yes (maximum flexibility)	Yes	Yes (Intrinsic to process)
Control of solid member diameter	Limited	Independent control	Independent control	Independent control
Member angle control*	0–90°	0–90°	0–90°	~50–90°
Fabrication area	0.1 m^2	0.25 m^2	0.005 m^2	~0.4 m^2
Thickness range	1–20 cm	1 mm–0.1 m	10– 100 μm	100 μm–5 cm
Nominal max. volume	0.02 m^3	1 m^3	10^{-6} m^3	0.02 m^3
Max no. unit cells through thickness.	~10	10′s	~10	~10
Min. unit cell size	~100 μm	<10 μm	<2 μm	<50 μm
Min. feature size	~10 μm	<1 μm	<<0.1 μm	<5 μm
Max. no. truss elements in a cubic volume	~4000	>10 000	~1000	~4000
Potential to grade properties	Limited	Yes (highest flexibility)	Yes	Yes
Possible base materials	Metals, polymers	Polymers	Polymers	Polymers
Post-processing material options	Annealing	Template for CVD/CVI, electroplating, casting, slurry coating, carbonization	Limited for very small structures: electroplating or CVD are possible	Template for CVD/CVI, electroplating, investment casting, slurry coating, carbonization
Rate of manufacture	Hours	Hours to days	Minutes to hours	Minutes
Potential for scalable manufacturing	Medium (single parts only)	Low (single parts only)	Low (single parts only)	High (>1 m^2/min for continuous process)

*(relative to horizontal).

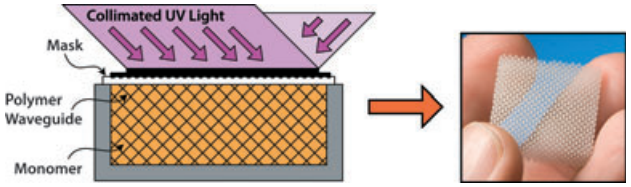

Fig. 8. Schematic representation of the process used to form micro-truss structures from self-propagating polymer waveguides (SPPW) and a prototypical structure formed by this process.[45]

load for conservativeness. For optimal structures in the buckling-dominated regime, $\sigma_{lb}=\sigma_{gb}$, resulting in

$$(t/l)=\frac{\pi^2\sqrt{3(1-\nu^2)}}{2}(a/l)^3.$$

The transition between buckling- and yielding-dominated regimes now occurs at:

$$\bar{\rho}_{trans}=\frac{8\sqrt{3(1-\nu^2)}}{\pi\sin\omega\cos^2\omega}\varepsilon_Y{}^2.$$

For a metal, $\bar{\rho}_{trans}\sim 0.002\%$. Hence, metallic hollow trusses are yielding-dominated in the entire range of feasible relative densities, with substantial benefits on the strength (Fig. 12). For applications exploiting the local plastic buckling modes of hollow trusses, such as energy absorption, the advantage is even more significant. The amount of energy dissipated in crushing a bar by global (Euler) buckling is insignificant compared to the amount of energy absorbed in local modes. The implication is that hollow truss lattice materials will exhibit unique properties as cores of impact resistant sandwich structures.[49]

The situation is qualitatively identical for ceramic materials, whereby the yield strength is replaced by a defect-sensitive fracture strength. See Section III(2)(B) for more details.

(B) Advantages of Small-Scale Architecture: The strength-density relation derived in Section III(2)(A) for both solid and hollow trusses is *length-scale independent*: proportional scaling of all dimensional geometric variables (truss bar length, l, radius, a, and wall thickness, t) has no effect on either relative density or specific strength. The fundamental assumption is that constituent material properties are themselves scale-independent. Although reasonable for wall thicknesses as small as a few microns, powerful strengthening effects will

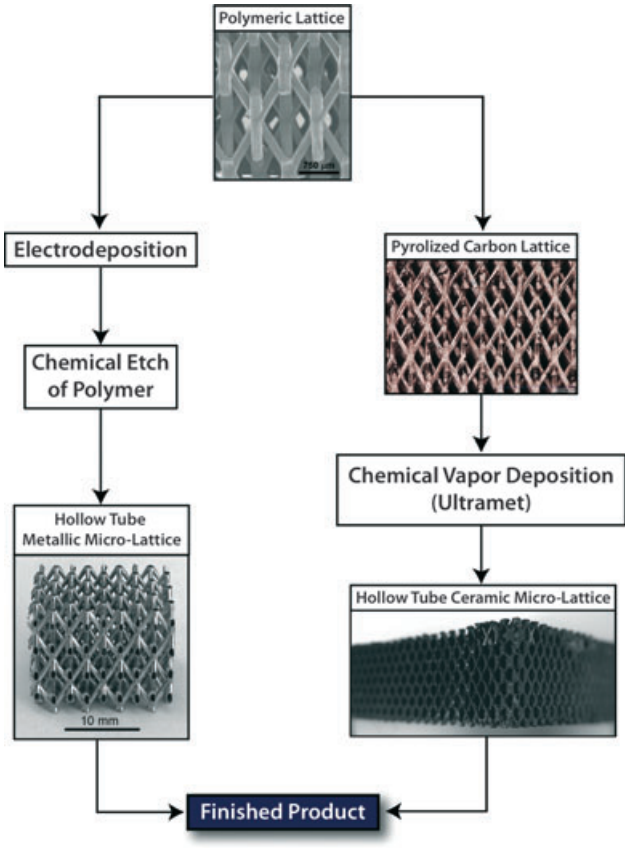

Fig. 10. Suitable fabrication routes for hollow tube metallic and ceramic micro-lattice structures (Images from Jacobsen *et al.*[45,157]).

emerge as sub-micron dimensions are approached. These recently documented effects arise from three phenomena: (a) yield strength elevation in metals due to strain gradient effects and/or (b) dislocation/surface interactions, and (c) fracture strength elevation in ceramics due to reduced average flaw size. Herein, we briefly review all the three mechanisms.

Scale Effects in Plasticity in the Presence of Strain Gradients: A large body of experimental investigations reveals the presence of size effects in plastic response that become more pronounced as the size of the sample (or the relevant length scale) approaches μm or sub-μm dimensions. Notable examples are the increase of indentation strength at shallower indentation depths,[53] increase in flow stress and

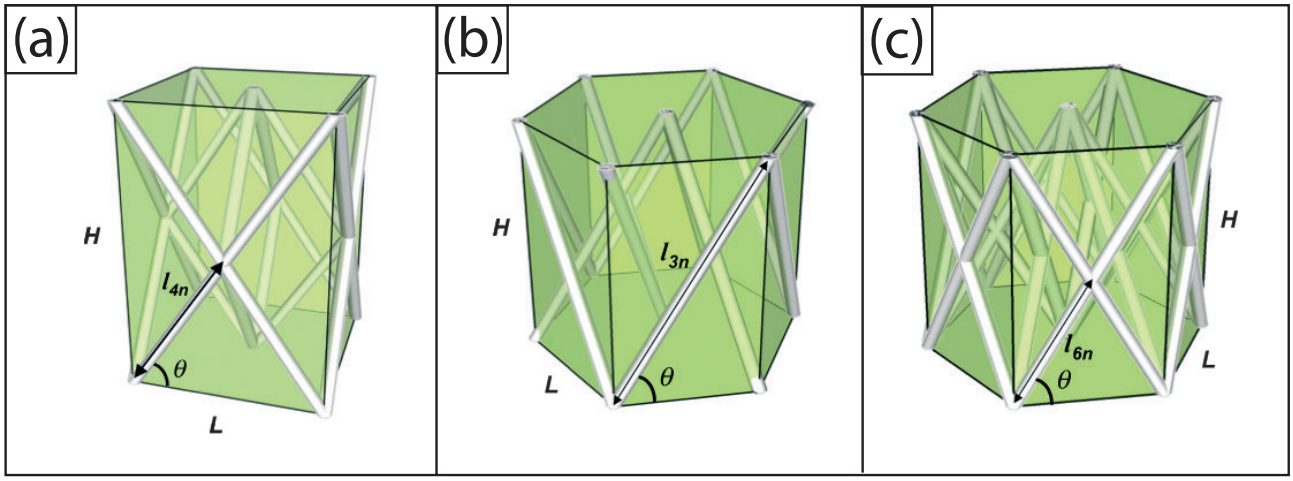

Fig. 9. Archetypal unit cell architectures with (a) 4-fold symmetry, (b) 3-fold symmetry, and (c) six-fold symmetry, as examples of structures that can be manufactured with the SPPW process depicted in Fig. 8 (from Jacobsen *et al.*[156]).

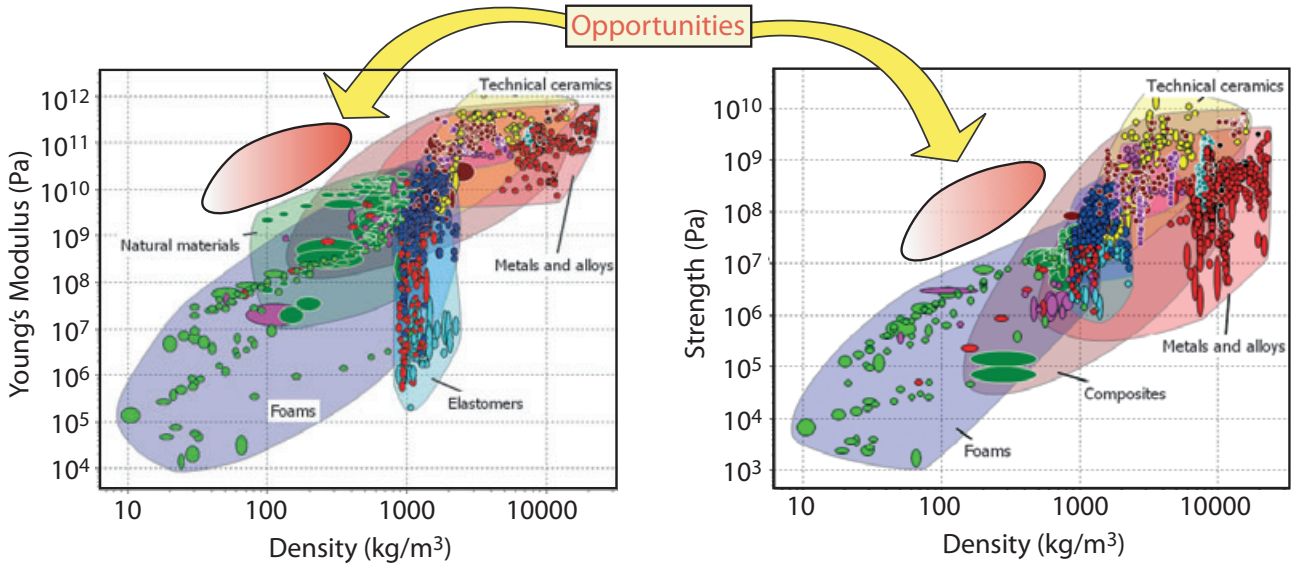

Fig. 11. Ashby charts for stiffness versus density, and compressive strength versus density, depicting all existing materials and emphasizing two target areas for micro-architected materials.

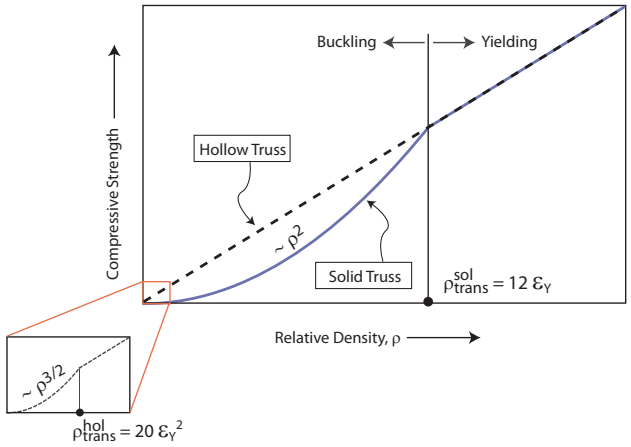

Fig. 12. Maximum compressive strength of solid and hollow metallic trusses. Notice that hollow trusses are yielding-dominated for any reasonable relative density.

hardening rate for thinner wires in torsion[54] and bending,[55] the classic Hall-Petch effect on the grain size dependence of flow stress,[56] and the increase in particle strengthening as the reinforcement size is reduced.[57] While these problems are vastly different, they all require a natural length scale for interpretation. A fundamental commonality in all the aforementioned situations is the presence of substantial plastic strain gradients during deformation. The development of constitutive laws that capture stress dependence on both strain and strain gradients is a natural modeling strategy. A number of strain gradient plasticity theories that reduce to the classic J_2 theory as the strain gradients are progressively reduced have been proposed over the past 25 years, most prominently by Fleck and Hutchinson,[58,59] and Nix and Gao.[60–62] The fundamental differences between the two theories in predicting experimental results were recently reviewed by Evans and Hutchinson.[63] Regardless of the differences, central to both theories is the concept of geometrically necessary dislocations (GND), initially introduced by Ashby.[64] Geometric considerations demonstrate that plastic strain gradients often require the storage of GNDs to maintain displacement compatibility. The GND density, ρ_G (total GND line length per unit volume) can be calculated once the active slip systems are identified. In an averaged sense, ρ_G can be related to the strain gradient, ε_p^*, through a natural length scale: $\rho_G \sim \varepsilon_p^*/\ell$, where ℓ is generally extracted from experimental results. Both theories predict hardening effects (and in the case of Fleck/Hutchinson, initial yield strength elevation) increasing with ρ_G.

Although a comprehensive strain gradient plasticity theory capable of capturing all the experimental phenomena while reducing to J_2 theory at large scale is still incomplete, there exists a general agreement on the marked effect of strain gradients on flow stress. These effects appear even at relative large sample sizes (~10 μm) and have the potential to substantially elevate the performance of micro-architected materials relative to their macro-scale counterparts. Although the lattice structures manufactured as described in Section III(1) (Fig. 10) will initially experience nearly zero strain gradients when loaded in compression and/or bending (all the truss members will uniformly compress or stretch), as the deformation progresses beyond first yield and the hollow truss members plastically buckle, substantial plastic strain gradients will arise. Although no initial yield strength elevation due to strain gradients is anticipated, both the collapse strength and the crushing energy (plastic dissipation) of micro-architected materials may be significantly higher than for conventional macro-scale materials. Recently, significant size effects have also been observed even in the absence of strain gradients, with further potential benefits to micro-architected materials. These effects are reviewed in the following subsection.

Size Effects in Plasticity in the Absence of Strain Gradients: Over the past 5 years, a multitude of room-temperature uniaxial compression and tension experiments have been performed on a wide range of single-crystalline metallic nano-pillars and nano-dogbones, including fcc metals (Ni and Ni-based superalloys,[65–67] Au,[68–71] Cu,[72–80] and Al[81,82]), bcc metals (W, Nb, Ta, and Mo[83–89]), hcp metals (Mg[90,91] and Ti[92]), tetragonal low-temperature metals (In[93]), Gum metal[94,95], nanocrystalline metals (Ni[96,97]), shape memory alloys (NiTi[98–102] and Cu-Al-Ni[103,104]), and a variety of metallic glasses[105–107]. For samples with nonzero initial dislocation densities (i.e., excluding whiskers and nano-fibers), a strong size effect on the flow strength was ubiquitously demonstrated as the sample size approached μm and sub-μm dimensions.[108] The compressive strength data for all single crystalline face-centered cubic (fcc) metals (Au, Al, Ni, and Cu) show a unique trend, suggesting the existence of a universal law of the form:

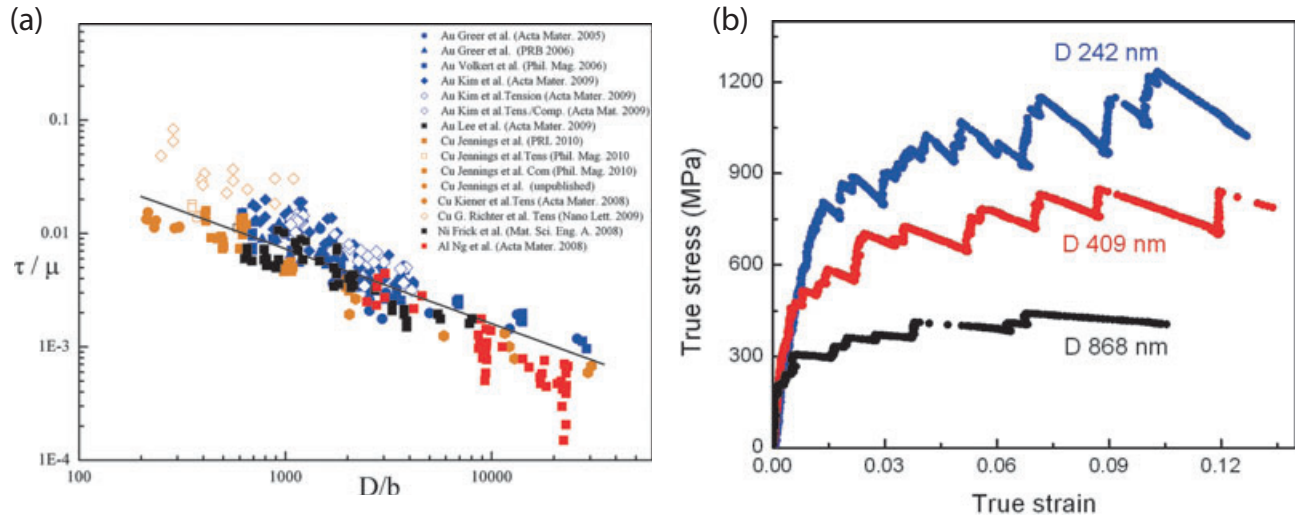

Fig. 13. Sample size effects on the flow stress in nanoscale experiments. (a) Shear flow stress (normalized with the shear modulus) VS sample diameter for a number of small-scale experiments on FCC metals reported in the literature. Resolving the stress on the relevant slip system and normalizing the sample diameter with the Burger's vector allow comparison of different metals on the same chart.[158] Reprinted from Greer and De Hosson (2011), with permission. (b) Compressive stress versus strain for uniaxial compression of single crystal Nb nano-pillars of different diameters (above each curve).[86]

$$\sigma_{res}/\mu = A(d/b)^{-m} \tag{7}$$

where μ is the shear modulus, σ_{res} is the resolved shear stress onto the {111}/<110> slip system, d is the pillar diameter, b is the Burgers vector, and A and m are constants (Fig. 13(a)). A similar observation was reported by Dou and Derby.[109] Based on the existing data for Au, Al, and Ni, A~0.71, and m~0.66. This exponent is nearly identical to those reported for nearly all other fcc micro- and nano-pillars where the samples contain initial dislocations.[108]

Figure 13(b) depicts some representative stress-strain curves for single crystalline Nb nano-pillars subjected to uniaxial compression.[86] The size-dependent strengthening effect cannot be explained through well-known thin-film mechanisms, such as grain size hardening,[110] the confinement of dislocations within a thin film by the substrate,[111] or the presence of strong strain gradients.[112] Intriguingly, unlike Taylor hardening, the flow strength does not appear to scale with the evolving density of mobile dislocations. Several models attempting to explain the causality between the declining dislocation density and attained strengths have been put forth. For example, the *dislocation starvation* model, first proposed by Greer and Nix[113] hypothesizes that the mobile dislocations inside a small nano-pillar have a greater probability of annihilating at a free surface than of interacting with one another, thereby shifting plasticity into nucleation-controlled regime.[66,68,69,114] Other models include source exhaustion hardening,[115,116] source truncation,[117,118] and weakest link theory.[116,118] The general commonality in all these theories is the representation of dislocation source operations in a discrete fashion, enabling an evaluation of the effect of sample size on the source lengths, and therefore on their operation strengths. Some of these models also capture the ubiquitously observed stochastic signature of the experimental results, showing either marginal dislocation storage[114,116,119] or no storage at all.[66,69,80]

The vast majority of samples for the nano-mechanical characterization described above have been produced by Focused Ion Beam (FIB). Figure 14 shows a number of examples. Unfortunately, the effect of the ion implantation introduced as a result of the FIB processing is not well characterized, and hinders an accurate interpretation of the experimentally observed size effects in plasticity. Although several investigators have reported Ga+ ion bombardbment damage resulting in altered microstructural features (e.g., dislocation sources,

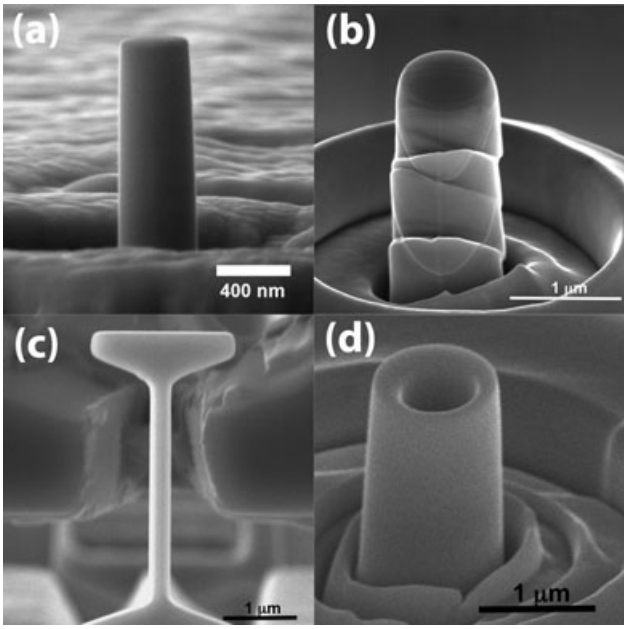

Fig. 14. SEM images of FIB-fabricated samples. (a) 400 nm nano-crystalline Ni-W nano-pillar. (b) Compressed 600 nm Nb pillar with significant slip offsets. (c) Typical dog-bone shaped tensile Au sample,[139,140] and (d) Mo anti-pillar with a hollow center.[159]

lattice rotations), attempts to attribute the observed strain hardening to these features have been inconclusive. Recent evidence (both experimental and computational, within and outside of the authors' groups) convincingly demonstrates that the size effect is a strong function of the initial dislocation density rather than the fabrication technique.[80,120] The size effects observed in the FIB-prepared specimens, for example, are identical to those obtained for the samples fabricated by a completely FIB-less technique, which contain similar initial dislocation densities.[121] Further, it has been reported that introducing dislocations into an initially pristine structure actually weakens rather that strengthens the sample.[122,123] In a recent computational study, it was reported that FIB-induced damage could contribute up to ~10% of the observed flow stress increase only for a particular size range between 500 nm and 1 μm, whereas for the larger and smaller specimens, the effects of the FIB on strength are marginal.[124]

Based on these arguments and the now ubiquitously reported presence of power-law size effects for all non-pristine pillars produced with or without the use of FIB, the authors are confident that the size effects are real and are *not* a function of the fabrication technique.

The ability to manufacture a macro-scale micro-architected material with a hollow truss topology characterized by truss wall thickness in the μm (and sub-μm) scale has the potential to exploit these beneficial size effects to achieve exceptional constituent materials properties. When combined with optimal design of the truss architecture, this approach should result in a macro-scale material with unprecedented specific strength. Admittedly, the metallic films deposited on the trusses will be polycrystalline, likely with a nanoscale grain size. The strengthening effects described above for fcc single crystals are much less understood in multi-grain surface-dominated small-scale systems. In fact, both homogeneous (grain boundaries, twin boundaries, etc.) and heterogeneous (i.e., phase boundaries, precipitate-matrix boundaries, free surfaces, and passivated surfaces) interfaces in size-limited features are crucial elements in the structural reliability of most modern materials. Yet very little work has been done on characterizing the combined effects of interfaces and surfaces—extrinsic (sample size in a surface-dominated structure) and intrinsic (microstructural features like grain boundaries, twin boundaries, phase boundaries, etc.)—on the mechanical response of materials. Furthermore, a vast majority of the above-mentioned experiments was conducted at room temperature, limiting our understanding of athermal versus thermal contribution to size-dependent strength. Significant efforts must be focused on investigating mechanical properties and identifying particular deformation mechanisms operating in boundary-containing metallic material systems with reduced dimensions (for example, nano-pillars containing two or three grains, twin boundaries, and homo- and heterogeneous nano-laminates). The knowledge of the specific deformation mechanisms as a function of feature size and initial microstructure will be essential for the design, manufacturing, and property control of new, revolutionary lightweight metallic micro-architected materials with unprecedented combinations of properties.

Fracture Strength Elevation in Ceramics at Small Scales: Ceramic thin films (e.g., carbon, silicon carbide, silicon nitride) possess yield strengths >10 GPa. Unless the constraining environment is such that crack growth is impeded (as would be the case for a uniform film adhered to a substrate and loaded in compression normal to the plane of the wafer), failure will generally occur by fracture. Linear elastic fracture mechanics predicts a fracture strength $\sigma_f \sim K_c^{solid}/\sqrt{a}$, with K_c^{solid} the fracture toughness of the constituent material and a the size of the largest crack. Assuming a statistical distribution of crack directions, mode I conditions will generally dominate the strength, whereby $K_c^{solid} = K_{Ic}^{solid}$ and a is the size of the largest crack oriented favorably to mode I propagation. The smaller the sample dimension, the smaller its largest crack. The implication is that the strength of a ceramic material will substantially increase as the sample length scale is reduced. As an example, a 5–10 μm thick polycrystalline diamond film deposited on a hollow truss might have[125] $a \sim 1\mu m$, $K_c \sim 4.6 MPa\sqrt{m}$, resulting in $\sigma_f \sim 4$ GPa. The relationship between the fracture toughness of a lattice and that of its constituent material has been recently elucidated by Fleck *et al.* for the case of planar lattices[126]: $K_{Ic}^{lattice}/K_{Ic}^{solid} \sim \rho^d\sqrt{\ell/a}$, with ρ the relative density of the lattice, ℓ the unit cell size, a the typical crack size in the constituent material, and the exponent d is a strong function of the lattice topology ($0.5 < d < 2$). Similar relationships can be derived for 3D lattices. If the architecture is properly chosen to minimize d, and assuming that the constituent crack size can be reduced together with the unit cell size, micro-architected lattice materials can have substantial fracture toughness, at a fraction of the weight of solid materials. At the same time, ceramics are exceptionally stiff (E~1TPa, for polycrystalline diamond[125]). Such strengths and stiffnesses are unattainable with any metallic system, offering ceramic micro-architected materials the potential to leap into currently unclaimed areas in a number of materials property charts. Importantly, the manufacturing technology described in Section III(1) is a key enabler for this vision: only an approach capable of manufacturing *large-scale* materials with *micron-level control* of the lattice architecture allows the base material to be deposited in the form of a sub-μm thin film. This has two enormous benefits: (i) it allows use of materials not available in the bulk (e.g., polycrystalline diamond), and (ii) it allows accurate control of the maximum flaw size, with enormous increases in the fracture strength relative to bulk values.

(3) Optimal Design Protocol for Micro-Architected Materials

The multi-step optimal design protocol presented in Section II in the context of large-scale periodic cellular structures is generally applicable to micro-architected materials. Although the general methodology is unchanged, a fundamental complexity emerges. *The bulk properties of micro-architected materials are a strong function of phenomena occurring across three length scales* (Fig. 15): a macroscopic level (bulk), a mesoscopic level (unit-cell) and a micro/nanoscopic level (the characteristic length scale of the constituent materials). Unique critical phenomena occur at each length scale, requiring experimental investigation. The size effects on plastic flow stress, strain hardening, and fracture strength (discussed above) are clearly micro/nano-scale phenomena, as are microstructure (and properties) anisotropy possibly arising from the film deposition process. Film thickness/microstructure variation along the truss members and details of the node topology—and their effects on the mechanical properties of the material—occur at the unit-cell level. The same length-scale can also affect the fracture strength, as variation in flaw distributions along members and around nodes can play a substantial role. Finally, the vast number of unit cells composing the bulk material may introduce large-scale effects previously unnoticed in macro-scale lattice materials: geometric imperfections (i.e., deviation from a perfect lattice) and the possible occurrence of buckling modes with characteristic length scale much larger than the unit cell level (and hence not captured with the type of analysis presented in Section II(2)) might play a significant role on the overall stiffness and strength of the bulk material. Novel characterization techniques and numerical strategies must be implemented to enable multi-scale studies. These are discussed below.

(4) Experimental Characterization of Micro-Architected Materials

(A) Macro-Scale Mechanical Characterization: At the macro-scale, conventional techniques traditionally employed for the characterization of large-scale lattice materials (and in fact, any other material) are perfectly adequate to analyze micro-architected materials. Traditional universal test frames (e.g., INSTRON, MTS) equipped with tensile, bending and shear fixtures can be used to measure stress-strain response in different loading scenarios and validate/calibrate analytical and numerical models for failure prediction.

(B) Micro-Scale Mechanical Characterization: As the unit cells of micro-architected materials can take many shapes and sizes, and several base materials can be used, the ideal device for mechanical characterization at this scale should have the following features: (i) be adaptable to samples of vastly different sizes and shapes; (ii) allow controlled displacement actuation and independent load measurement;

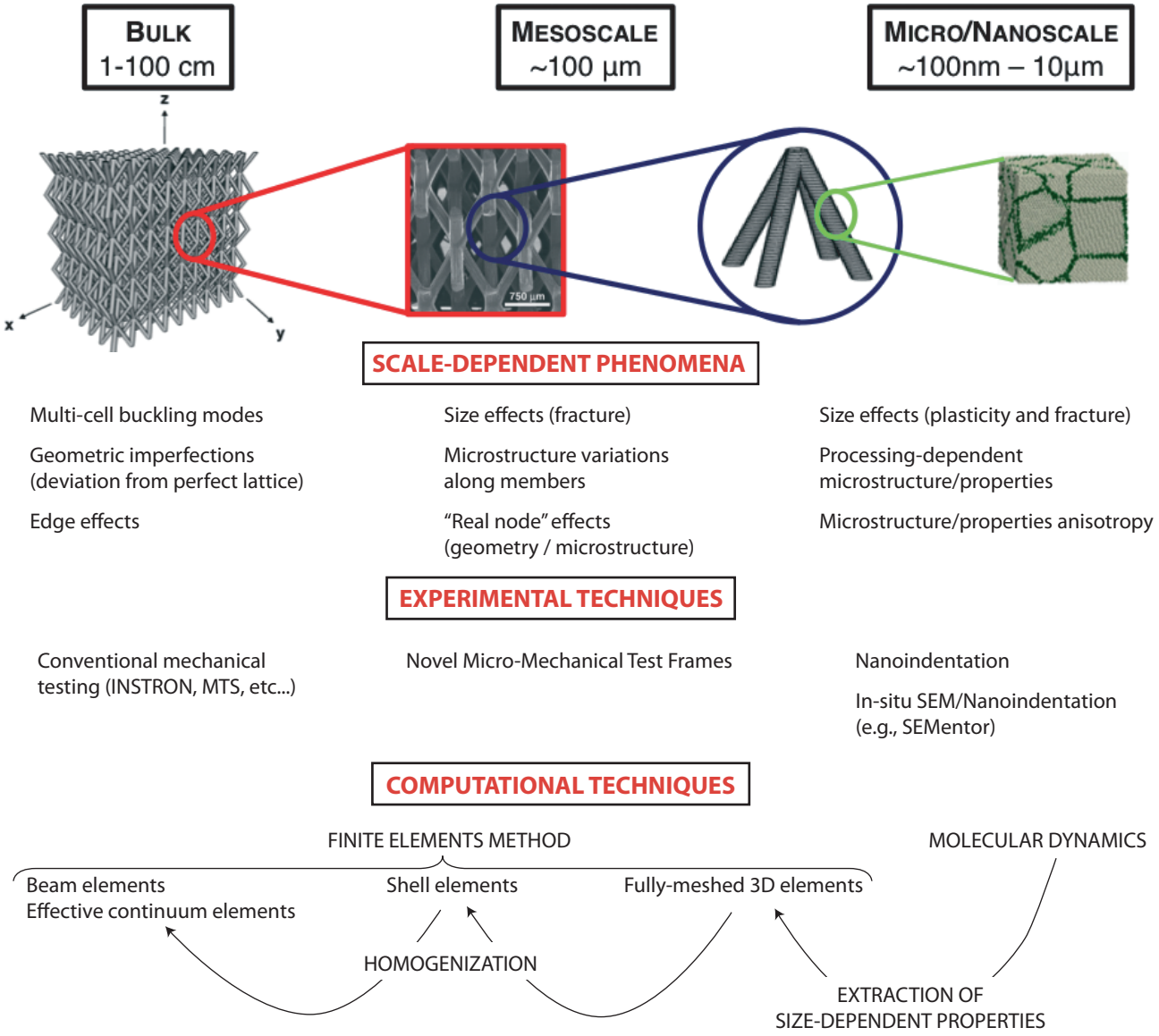

Fig. 15. Expected phenomena, mechanical characterization tools and computational techniques for the three length-scales of interest in micro-architected materials. (SEM images from Jacobsen *et al.*[45,160])

(iii) be capable of extreme force resolution (~1–100 nN) and range (~1 N), displacement resolution (~10–100 nm) and range (1–10 mm); and (iv) allow optical (or SEM) access to the test coupon with potential for strain mapping (via Digital Image Correlation). Hybrid micro-test frames, encompassing a MEMS force sensor and an off-chip displacement actuator, are necessary to meet the requirements listed above. A number of such devices have been developed in the past two decades.[127,128] An economical and versatile device, capable of covering the entire range of force and displacement described above, has been recently introduced by one of the authors (Fig. 16).[129] In the proposed design, the sensor is a micro-fabricated Silicon double-ended tuning fork (DETF), whose working principle is the change in natural frequency of vibration in a pair of parallel and connected beams upon application of an external axial force. DETF sensors deflect axially rather than laterally, hence exhibiting essentially infinite stiffness relative to the sample being tested and exceptional force range (in the Newton range). This is in stark contrast with the more commonly employed capacitive or visual force detection schemes, in which load cell and sample have comparable compliance. At the same time, the strong dependence of the natural frequency of a beam on the axial load and the extreme precision available in frequency measurement (a change of a fraction of a Hertz is easily detected in a 100 kHz signal) grant the device nN resolution. Samples of different geometry can be handled with micro-fabricated custom fixtures, enabling a variety of testing conditions (bending, compression, tension, etc.…).

(C) Nanoscale Mechanical Characterization: Uniaxial Mechanical Testing at the Nanoscale: The two best-established techniques for nanoscale mechanical characterization are Atomic Force Microscopy (AFM) and Nanoindentation. The former controls the displacement through a piezo-actuator and senses the force through the deflection of a micro-cantilever, typically measured optically. Although extreme force and deflection resolutions are possible,[1,130–132] the force range is small, on the order of a few pico-Newtons, with a vertical distance resolution smaller than ~0.1 nm. Such a small load range limits the applicability of AFM to the characterization of stiff materials (e.g., metals and ceramics). The mechanical properties of stiff materials can be well characterized by nanoindentation, whose premise involves forcing a generally sharp diamond indenter tip into the surface of a material, while measuring the imposed force, the corresponding displacement of the indenter, and in some cases, the contact stiffness.[62,133–138] Nanoindenters are inherently

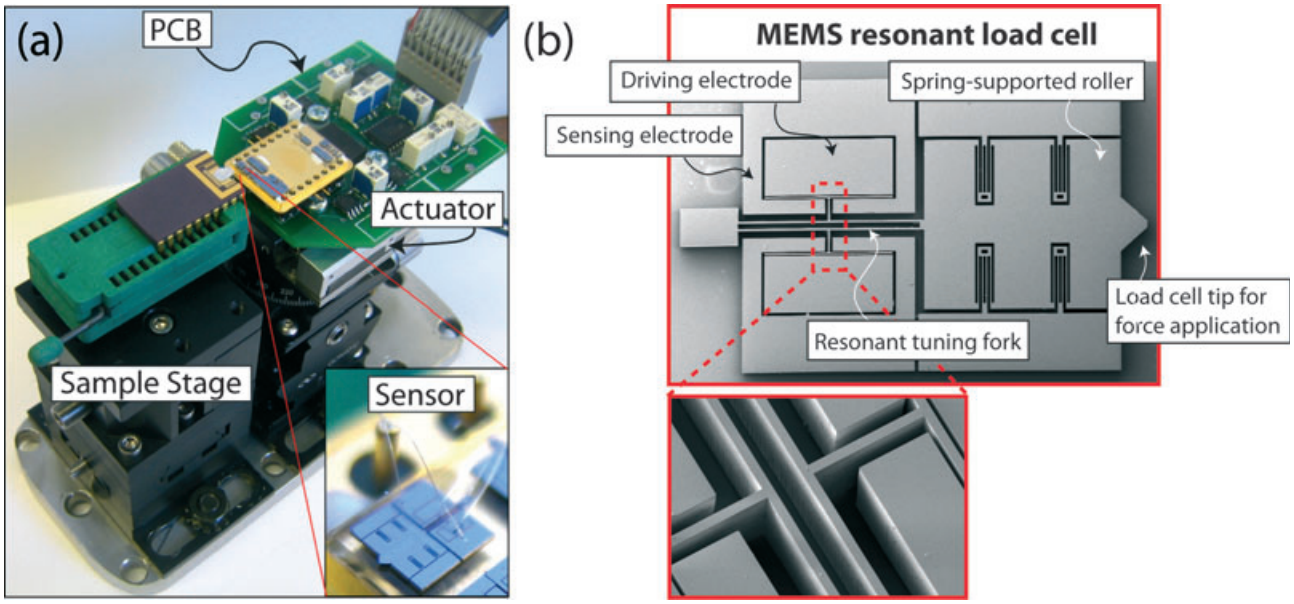

Fig. 16. (a) Micro-mechanical test frame (μ-MTF) for unit-cell level characterization. The displacement actuator is a commercially available nano-stage, while the load cell (inset) is microfabricated. (b) Detail of the microfabricated load cell (From Torrents *et al.*[129] and Azgin *et al.*[161])

load-controlled instruments, where the load is applied through an electromagnetic coil assembly, and the displacement is measured by capacitive gages. Typical modern-day nanoindenters have load resolution of several nano-Newtons and sub-nanometer displacement resolution. From a measurement of the indentation depth, the local hardness, H, of the material is readily accessed, and the yield strength is generally estimated as $\sigma_Y \approx H/3$. Obtaining more detailed mechanical information is unfortunately very difficult: the stress and strain fields induced by the indenter are complex and tri-axial, rendering the interpretation of experimental results challenging. Carving nanoscale samples in the shape of pillars or dog-bones addresses this difficulty, by enabling the introduction of nearly uniaxial stress and strian fields (see Section III(2)(B)). To allow *in-situ* observation of the sample deformation, nanoindenters have been coupled with electron microscopes. A unique such instrument (called the "SEMentor") was recently developed by one of the authors.[139,140] The SEMentor is comprised of a nanomechanical module, similar to the DCM assembly of a commercial Agilent nanoindenter, inside of a SEM. The former offers a precise control and high resolution of load (~1 nN) and displacement (<1 nm) and their rates, as well as contact stiffness during the experiment, while the latter allows for visualization of the process. Custom-made grips were fabricated to conduct nanoscale *in-situ* experiments in uniaxial compression and tension. Uniaxial tensile investigations will be essential in determining nanoscale yield and ultimate tensile strength and fracture toughness of nanoscale materials, as well as in elucidating the origins of tension/compression asymmetry likely to be observed in nanoscale polycrystalline samples. All these features are critically important to the development of micro-architected materials. Furthermore, this *in-situ* testing technique will allow correlation of the macroscopic stress-strain behavior with some microstructural activity by direct observation of, for example, the dislocation glide "avalanches" manifested by multiple slip lines, shear offsets, and phase delamination (if any).

Microstructural Characterization: A key analytical technique allowing direct observation of dislocations and their interactions with various boundaries and surfaces is High Resolution Transmission Electron Microscopy (HR-TEM). While, of course, the post-mortem TEM analysis is not capable of providing any information about the mobile defect activity, it is powerful in revealing the post-deformation microstructure, i.e., the evolved dislocation networks, the final grain configurations, and most importantly it sheds light on the particular interactions of dislocations with the individual interfaces and surfaces in the deformed samples. This information is useful in uncovering some of the fundamental mechanisms that might have operated during deformation of these nano-volumes with specified interfaces.

(5) Numerical Modeling of Micro-Architected Materials

(A) Continuum-Based Approaches (Finite Elements Analysis): Once the properties of the thin film base materials are known (including their size effects), traditional contin-

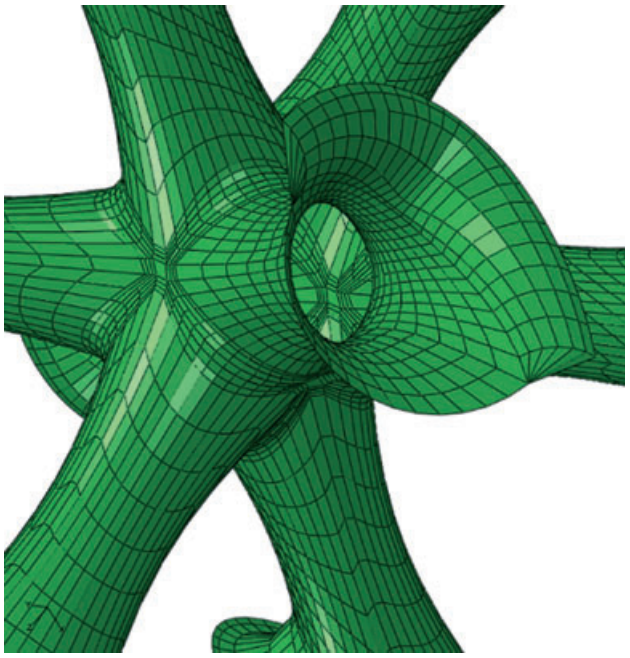

Fig. 17. Example of Finite Elements mesh for micro-architected hollow truss structures. Node fillet radii, nonuniform wall thicknesses, noncircular cross-sections and bar tapers are parametrically defined with geometric modeling tools, for efficient integration with optimization algorithms.

uum finite elements approaches can be used to extract both the unit cell properties as well as the averaged bulk properties of micro-architected materials. Although the numerical tools are identical to those used for large-scale lattice materials (see Section II), some additional steps must be taken to merge the unit cell and the bulk length scales (Fig. 15).

Finite Elements Modeling of Individual Trusses and Unit Cells: Individual hollow truss members and unit cells can be modeled with shell elements and/or solid elements. Besides validating the analytical predictions for an ideal structure, FE modeling must quantify the effect of three potentially critical factors on stiffness, strength, ductility, and collapse mechanisms. *(i) Geometric non-uniformities* (e.g., curviness in nominally straight truss members, non-ideal node size and shape, and wall thickness variations along members and within nodes). *(ii) Heterogeneity and anisotropy in materials properties* (arising from variations in grain size and texture along the trusses and around the nodes). *(iii) Interface strength and toughness in multi-materials systems* (e.g., a ceramic film deposited on a metallic wall). These phenomena are in principle present in large-scale lattice structures as well, but their effect on the overall properties is typically negligible. Geometric algorithms for automatic meshing are essential to capture point (i) above (Fig. 17).

Large-Scale (Multi-Cells) Finite Elements Modeling: The vast difference between the unit cell and the bulk scales requires numerical strategies for efficient modeling. Generally, the plethora of Finite Elements results extracted from the fully meshed unit-cell models described above must be condensed into a lower-order model (homogenization). Two sequential approaches can be envisioned, in increasing order of complexity and computational efficiency: (a) beam-elements unit-cell model; (b) effective 3D solid elements model. For approach (a), each unit cell is modeled with a number of beam elements and the effects of nodal size/shape and local buckling that are lost in transitioning from shell to beam elements can be incorporated by introducing fictitious (non-uniform) stress-strain response for the material. Approach (b) follows homogenization procedures similar to those implemented for large-scale period core sandwich panels.[26,141] The challenge is to define the constitutive behavior of the material in a way that a single solid element (possibly with size spanning several unit cells) elastically and plastically deforms consistently with buckling phenomena that are dominated by length scales of the order of the unit cell size, truss radius and wall thickness.

(B) Atomistic Approaches (Molecular Statics and Dynamics): Standard molecular dynamics (MD) and molecular statics (MS) techniques can be used to develop quantitative predictions of the elastic behavior of brittle ceramics and the elasto-plastic behavior of ductile metals and nanostructured composites of ductile and brittle materials. The Embedded Atom Method (EAM) potential[142] and the Modified EAM (MEAM) potential[143] are appropriate for metals, whereas materials with significant angular bonding (such as some ceramics) require dedicated MEAM potentials.[144] Molecular statics (MS) approaches are adequate for stiffness calculations, both in single crystal and nanocrystalline samples, and enable investigation of the role of all strain components on grain size and orientation at T~0K (this is acceptable as stiffness is not expected to be a strong function of temperature). If necessary, temperature effect can be quantified with MD simulations at non-zero temperature. Prediction of the plastic behavior of micro-architected materials at the nanoscale is significantly more challenging, as significant size and orientation effects might dominate strength and ductility. Controlled defects can be introduced to examine trade-offs between homogeneous and heterogeneous dislocation and void nucleation. As plastic flow is highly temperature dependent, MS is inadequate for elasto-plastic investigations, and MD simulations must be performed at nonzero temperature (typically at T~273 K). A substantial challenge is bridging the simulation and experimental time scales: computational resources demand strain rates $>10^6\,s^{-1}$ for all MD simulations, whereas experiments typically take place at rates of $1\,s^{-1}$ or less. To avoid recoding fictitious strain rate effects in the data, high strain rate MD simulations must be extrapolated to lower strain rates, possibly using mechanism-based modeling. Validation of these calculations with nanoscale experiments (Section III(4)(C)) is critical to ensure that deformation mechanisms unveiled by the MD simulations persist even at much lower strain rates. MD capabilities to accurately predict the initial yield point have been well established. Quantitatively capturing phenomena subsequent to failure initiation (e.g., hardening and ultimate failure) is less straightforward. Once again, nanomechanical experiments will be essential to validate and supplement MD models. MD and FEM analyses can be interfaced *off-line* with phenomenological constitutive laws: such laws are informed by MD (e.g., yield strength VS sample size) and can be easily imported in commercial FE packages (either directly or via user-defined subroutines). Naturally, combining MD numerical schemes at the nanoscale with FE calculations at the micro and macro scale in *real-time* in a truly multi-scale algorithm is the Holy Grail of computational mechanics. After decades of research in multi-scale mechanics, this is still a daunting task. Nonetheless, *off-line* combinations of atomistic simulations at the nanoscale and Finite Elements and analytical continuum mechanics at the micro/macro-scale have been capable of macro-scale properties predictions.[145] Experimental results as those described in Section III(4) are often necessary for model calibration.

In addition to MD and MS simulations, Discrete Dislocations Simulations (DDS) have been introduced to compute the effect of dislocation motion and interaction on plastic flow in crystals.[146–148] These models generally utilize a FE continuum framework to solve for stresses, strains and displacements, and treat dislocations as singularities, which both affect and are affected by the global strain and stress fields. Dislocations motion is governed by the Peach-Koehler equation and standard dislocation-dislocation interaction laws. Dislocation sources like Frank-Read and single-arm sources are introduced at statistically random locations. These models (both in 2D and 3D) are computationally more efficient than full-scale MD simulations, but have not yet fully succeeded in duplicating key aspects of the experimentally measured size effects in plasticity.[149]

(C) Optimization Algorithms: The large number of variables in the optimal design of micro-architected materials, coupled with the possible difficulty in obtaining closed-

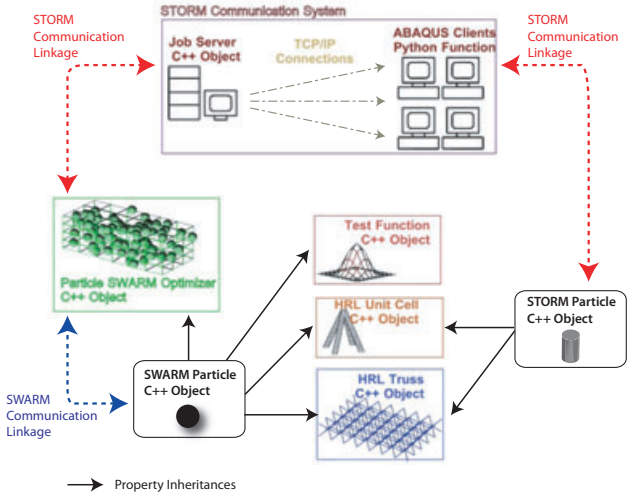

Fig. 18. Schematic of a possible efficient optimization code for the optimal design of complex micro-architected materials.[36] The optimizer can be coupled with commercial Finite Elements packages for on-line fully numerical optimization.

form solutions for some of the objectives and constraints, require an optimization procedure more sophisticated than that typically used for the optimization of macro-scale structures (Section II). Importantly, most of the structural optimization work performed to date assumes that the *constituent material(s)* and the *architecture* of the cellular structure is decided *a priori,* and the optimizer must simply select the best values for all the *geometric parameters* that define that architecture (e.g., unit-cell size, truss angle, wall thickness). A large number of architectures were independently studied at the macroscopic scales.[11,12,15,16,150] Standard quadratic optimizers were typically used, and relied on close-form expressions for the objective function and all the constraints. Although easy and convenient, this approach might be unsuitable for the optimization of micro-architected multifunctional materials, for two reasons: (i) complex geometric features (e.g., details of the node architecture) might strongly affect stress and strain distributions, and hence impede close-form expressions of objective and constraints, and (ii) a large number of local optima might appear, which could confuse quadratic optimizers. Discrete optimizers (e.g., genetic or particle swarm optimizers) do not require close-form expressions for objectives and constraints and are rather insensitive to local minima. Unfortunately, their robustness and efficiency are not as good as for gradient-based algorithms. A discrete optimization protocol that allows on-line interaction with a commercial Finite Elements program for objective function evaluation is schematically described in Fig. 18.[36] The on-line integration of FE analyses within the optimization loops is extremely resource-intensive. Although novel software technology (e.g., Microsoft HPC) will help, this remains a key bottleneck in the optimization process.

Ultimately, to take full advantage of the nearly infinite freedom in designing with micro-architected materials, the topological architecture of the material should be itself a variable in the optimization process. Topology optimization algorithms were developed over the past couple of decades,[151–154] with the scope of defining the ideal arrangement of two or more phases of matter (one might be air to define a cellular solid) to achieve extremal values in one or more macroscopic properties. These algorithms are naturally more complex and resource-intensive than the simple procedure described in Section II. In addition, although exceptionally interesting and unexpected results might occur (e.g., when the Kagome structure was identified by Torquato's group as an ideal stiff and statically determinate lattice,[155] spearheading dozens of studies on its mechanical properties and technological importance,[28,30,150]) in many cases the resulting topologies are nearly impossible to manufacture. Nonetheless, incorporation of topology optimization concepts within the computational framework described in Section II is a promising way to explore a massive design space.

IV. Conclusions

Periodic cellular materials and structures have been extensively investigated over the past decade for a large number of multifunctional applications. A common optimal design protocol was successfully adopted in several studies to select the geometry, architecture, and base material that maximizes the relevant objective function(s). The protocol employs a combination of analytical, numerical, and experimental techniques, and was reviewed herein in the context of mechanical and thermo-mechanical structures. We extended this concept to the multi-scale design of a micro-architected material. Enabling this vision are newly available manufacturing approaches for suitable periodic cellular architectures with unit cell sizes in the sub-millimeter scale and constituent material characteristic length in the micro/nano scale. The resulting micro-architected material is characterized by three different length scales: a bulk scale (~1–100 cm), a unit-cell scale (~100 μm–1 mm) and a constituent material scale (~100 nm–10 μm). We surmise that micro-architected materials will possess unique superior mechanical properties (primarily specific stiffness and strength), by exploiting recently observed size effects at the micro and nano scales. Extending optimal design protocols for large-scale periodic cellular structures to the case of micro-architected materials entails the added difficulty that bulk mechanical properties are now a strong function of physical phenomena occurring at three different length scales. Existing modeling tools must be adapted to handle such difficulty. We briefly reviewed the state-of-the-art in small-scale mechanical characterization and numerical modeling and concluded that the necessary techniques are sufficiently mature to underpin the development of micro-architected materials. As the length scale ℓ of a periodic cellular structure shrinks to sub-millimeter dimensions, and the number of unit cells in the bulk material increases as ℓ^{-3}, the difference between a *structure* and a *material* gets progressively blurred: in this sense, micro-architected materials represent a new class of materials, characterized by a unique variable amenable to optimization: the *topological architecture*. We hope that this overview will stimulate intense research efforts aimed developing new micro-architected materials with properties outside of the boundaries of current materials properties spaces into new, previously unclaimed regions.

Acknowledgments

The authors are grateful to DARPA for financial support through grant no. W91CRB-10-C-0305 on Materials with Controlled Microstructural Architecture (Judah Goldwasser, program manager). LV acknowledges partial funding from the California-Catalonia Engineering Program. JRG acknowledges the financial support from NSF CAREER Award (DMR-0748267) and ONR Grant no. N000140910883. WBC and AJJ also acknowledge prior DARPA support through contract no. W911NF-08-C-0038 and internal support funds from HRL. The authors dedicate this article to the memory of Anthony G. Evans, who inspired and directed much of the work on periodic cellular materials. His leadership, enthusiasm, and mentorship are dearly missed.

References

[1]L. J. Gibson and M. F. Ashby, *Cellular Solids: Structure and Properties*. Cambridge University Press, Cambridge, UK, 1999.

[2]M. F. Ashby, A. G. Evans, N. A. Fleck, L. J. Gibson, J. W. Hutchinson, and H. N. G. Wadley, Metal Foams: A Design Guide. Butterworth-Heinemann, Oxford, UK, 2000.

[3]T. J. Lu, L. Valdevit, and A. G. Evans, "Active Cooling by Metallic Sandwich Structures With Periodic Cores," *Prog. Mater. Sci.*, **50** [7] 789–815 (2005).

[4]A. G. Evans, J. W. Hutchinson, N. A. Fleck, M. F. Ashby, and H. N. G. Wadley, "The Topological Design of Multifunctional Cellular Metals," *Prog. Mater. Sci.*, **46** [3-4] 309–27 (2001).

[5]H. N. G. Wadley, "Cellular Metals Manufacturing," *Adv. Eng. Mater.*, **4** [10] 726–33 (2002).

[6]H. N. G. Wadley, N. A. Fleck, and A. G. Evans, "Fabrication and Structural Performance of Periodic Cellular Metal Sandwich Structures," *Compos. Sci. Technol.*, **63** [16] 2331–43 (2003).

[7]H. Bart-Smith, A. F. Bastawros, D. R. Mumm, A. G. Evans, D. J. Sypeck, and H. N. G. Wadley, "Compressive Deformation and Yielding Mechanisms in Cellular Al Alloys Determined Using X-ray Tomography and Surface Strain Mapping," *Acta Mater.*, **46** [10] 3583–92 (1998).

[8]H. Bart-Smith, J. W. Hutchinson, and A. G. Evans, "Measurement and Analysis of the Structural Performance of Cellular Metal Sandwich Construction," *Int. J. Mech. Sci.*, **43** [8] 1945–63 (2001).

[9]A. F. Bastawros, H. Bart-Smith, and A. G. Evans, "Experimental Analysis of Deformation Mechanisms in a Closed-Cell Aluminum Alloy Foam," *J. Mech. Phys. Solids*, **48** [2] 301–22 (2000).

[10]H. Bart-Smith, J. W. Hutchinson, N. A. Fleck, and A. G. Evans, "Influence of Imperfections on the Performance of Metal Foam Core Sandwich Panels," *Int. J. Solids Struct.*, **39** [19] 4999–5012 (2002).

[11]N. Wicks and J. W. Hutchinson, "Optimal Truss Plates," *Int. J. Solids Struct.*, **38** [30–31] 5165–83 (2001).

[12]L. Valdevit, J. W. Hutchinson, and A. G. Evans, "Structurally Optimized Sandwich Panels With Prismatic Cores," *Int. J. Solids Struct.*, **41** [18–19] 5105–24 (2004).

[13]L. Valdevit, Z. Wei, C. Mercer, F. W. Zok, and A. G. Evans, "Structural Performance of Near-Optimal Sandwich Panels With Corrugated Cores," *Int. J. Solids Struct.*, **43** [16] 4888–905 (2006).
[14]N. Wicks and J. W. Hutchinson, "Performance of Sandwich Plates With Truss Cores," *Mech. Mater.*, **36** [8] 739–51 (2004).
[15]F. W. Zok, H. Rathbun, M. He, E. Ferri, C. Mercer, R. M. McMeeking, and A. G. Evans, "Structural Performance of Metallic Sandwich Panels With Square Honeycomb Cores," *Philos. Mag.*, **85** [26–27] 3207–34 (2005).
[16]F. W. Zok, H. J. Rathbun, Z. Wei, and A. G. Evans, "Design of Metallic Textile Core Sandwich Panels," *Int. J. Solids Struct.*, **40** [21] 5707–22 (2003).
[17]F. W. Zok, S. A. Waltner, Z. Wei, H. J. Rathbun, R. M. McMeeking, and A. G. Evans, "A protocol for Characterizing the Structural Performance of Metallic Sandwich Panels: Application to Pyramidal Truss Cores," *Int. J. Solids Struct.*, **41** [22–23] 6249–71 (2004).
[18]L. Valdevit, A. Pantano, H. A. Stone, and A. G. Evans, "Optimal Active Cooling Performance of Metallic Sandwich Panels With Prismatic Cores," *Int. J. Heat Mass Transfer*, **49** [21–22] 3819–30 (2006).
[19]L. Valdevit, N. Vermaak, F. W. Zok, and A. G. Evans, "A Materials Selection Protocol for Lightweight Actively Cooled Panels," *J. Appl. Mech.*, **75**, 061022 (2008).
[20]N. Vermaak, L. Valdevit, and A. G. Evans, "Influence of Configuration on Materials Selection for Actively Cooled Combustors," *J. Propul. Power*, **26** [2] 295–302 (2010).
[21]N. Vermaak, L. Valdevit, and A. G. Evans, "Materials Property Profiles for Actively Cooled Panels: An Illustration for Scramjet Applications," *Metall. Mater. Trans. A.*, **40A** [4] 877–90 (2009).
[22]C. S. Roper, "Multiobjective Optimization for Design of Multifunctional Sandwich Panel Heat Pipes With Micro-Architected Truss Cores," *Int. J. Heat Fluid Flow*, **32**, 239–48 (2011).
[23]H. J. Rathbun, D. D. Radford, Z. Xue, M. Y. He, J. Yang, V. Deshpande, N. A. Fleck, J. W. Hutchinson, F. W. Zok, and A. G. Evans, "Performance of Metallic Honeycomb-Core Sandwich Beams Under Shock Loading," *Int. J. Solids Struct.*, **43** [6] 1746–63 (2006).
[24]M. T. Tilbrook, V. S. Deshpande, and N. A. Fleck, "The Impulsive Response of Sandwich Beams: Analytical and Numerical Investigation of Regimes of Behaviour," *J. Mech. Phys. Solids*, **54** [11] 2242–80 (2006).
[25]H. N. G. Wadley, K. P. Dharmasena, M. Y. He, R. M. McMeeking, A. G. Evans, T. Bui-Thanh, and R. Radovitzky, "An active Concept for Limiting Injuries Caused by Air Blasts," *Int. J. Impact Eng.*, **37** [3] 317–23 (2010).
[26]Z. Y. Xue and J. W. Hutchinson, "Crush Dynamics of Square Honeycomb Sandwich Cores," *Int. J. Numer. Meth. Eng.*, **65** [13] 2221–45 (2006).
[27]L. H. Han, T. J. Lu, and A. G. Evans, "Optimal Design of a Novel High Authority SMA Actuator," *Mech. Adv. Mater. Struct.*, **12** [3] 217–27 (2005).
[28]R. G. Hutchinson, N. Wicks, A. G. Evans, N. A. Fleck, and J. W. Hutchinson, "Kagorne Plate Structures for Actuation," *Int. J. Solids Struct.*, **40** [25] 6969–80 (2003).
[29]T. J. Lu, J. W. Hutchinson, and A. G. Evans, "Optimal Design of a Flexural Actuator," *J. Mech. Phys. Solids*, **49** [9] 2071–93 (2001).
[30]S. Lucato, J. Wang, P. Maxwell, R. M. McMeeking, and A. G. Evans, "Design and Demonstration of a High Authority Shape Morphing Structure," *Int. J. Solids Struct.*, **41** [13] 3521–43 (2004).
[31]N. Wicks and J. W. Hutchinson, "Sandwich Plates Actuated by a Kagome Planar Truss," *J. Appl. Mech.-Trans. Asme*, **71** [5] 652–62 (2004).
[32]W. D. Macdonald and T. W. Eagar, "Transient Liquid-Phase Bonding," *Annu. Rev. Mater. Sci*, **22**, 23–46 (1992).
[33]Wall-Colmonoy Corporation. Available at http://www.wallcolmonoy.com
[34]D. T. Queheillalt and H. N. G. Wadley, "Titanium alloy Lattice Truss Structures," *Mater. Des.*, **30** [6] 1966–75 (2009).
[35]S. J. Johnson, B. Tryon, and T. M. Pollock, "Post-Fabrication Vapor Phase Strengthening of Nickel-Based Sheet Alloys for Thermostructural Panels," *Acta Mater.*, **56** [17] 4577–84 (2008).
[36]S. W. Godfrey, "Optimal Design of Orthotropic Fiber-Composite Corrugated-Core Sandwich Panels Under Axial Compression"; MS Thesis, Mechanical and Aerospace Engineering, University of California, Irvine, (2010).
[37]B. P. Russell, V. S. Deshpande, and H. N. G. Wadley, "Quasi-Static Deformation and Failure Modes of Composite Square Honeycombs," *J. Mech. Mater. Struct.*, **3** [7] 1315–40 (2008).
[38]A. P. Mouritz and B. N. Cox, "A Mechanistic Interpretation of the Comparative In-Plane Mechanical Properties of 3D Woven, Stitched and Pinned Composites," *Compos. Part A - Appl. S.*, **41** [6] 709–28 (2001).
[39]V. S. Deshpande, N. A. Fleck, and M. F. Ashby, "Effective Properties of the Octet-Truss Lattice Material," *J. Mech. Phys. Solids*, **49** [8] 1747–69 (2001).
[40]N. Vermaak, "Thermostructural Design Tools for Hypersonic Vehicles," Ph.D. Thesis, Materials Department, University of California, Santa Barbara, 2010.
[41]D. Queheillalt and H. Wadley, "Cellular Metal Lattices With Hollow Trusses," *Acta Mater.*, **53** [2] 303–13 (2005).
[42]Q. Li, E. Y. Chen, D. R. Bice, and D. C. Dunand, "Mechanical Properties of Cast Ti-6Al-2Sn-4Zr-2Mo Lattice Block Structures," *Adv. Eng. Mater.*, **10** [10] 939–42 (2008).
[43]F. P. W. Melchels, J. Feijen, and D. W. Grijpma, "A Review on Stereolithography and its Applications in Biomedical Engineering," *Biomaterials*, **31** [24] 6121–30 (2010).
[44]H.-B. Sun and S. Kawata, "Two-Photon Photopolymerization and 3D Lithographic Microfabrication," pp. 169–273 in *NMR, 3D Analysis, Photopolymerization*, Vol. 190. Edited by N. Fatkullin. Springer, Berlin, Germany, 2004.
[45]A. J. Jacobsen, W. Barvosa-Carter, and S. Nutt, "Micro-Scale Truss Structures Formed From Self-Propagating Photopolymer Waveguides," *Adv. Mater.*, **19** [22] 3892–6 (2007).
[46]A. J. Jacobsen, J. A. Kolodziejska, R. Doty, K. D. Fink, C. Zhou, C. S. Roper, and W. B. Carter, "Interconnected Self-Propagating Photopolymer Waveguides: An Alternative to Stereolithography for Rapid Formation of Lattice-Based Open-Cellular Materials" in *Twenty First Annual International Solid Freeform Fabrication Symposium - An Additive Manufacturing Conference*, University of Texas, Austin (2010).
[47]J. Banhart, "Manufacture, Characterisation and Application of Cellular Metals and Metal Foams," *Prog. Mater. Sci.*, **46**, 559–632 (2001).
[48]M. Scheffler and P. Colombo, "*Cellular Ceramics: Structure, Manufacturing, Properties and Applications*. WILEY, Weinheim, 2005.
[49]A. G. Evans, M. Y. He, V. S. Deshpande, J. W. Hutchinson, A. J. Jacobsen, and W. B. Carter, "Concepts for Enhanced Energy Absorption Using Hollow Micro-Lattices," *Int. J. Impact Eng.*, **37** [9] 947–59 (2010).
[50]A. Jacobsen, S. Mahoney, and W. Carter, "Vitreous Carbon Micro-Lattice Structures," *Carbon*, **49**, 1023–32 (2011).
[51]V. S. Deshpande and N. A. Fleck, "Collapse of Truss Core Sandwich Beams in 3-Point Bending," *Int. J. Solids Struct.*, **38** [36–37] 6275–305 (2001).
[52]H. G. Allen and P. S. Bulson, "*Background to Buckling*." McGraw-Hill, London, 1980.
[53]M. R. Begley and J. W. Hutchinson, "The Mechanics of Size-Dependent Indentation," *J. Mech. Phys. Solids*, **46** [10] 2049–68 (1998).
[54]N. A. Fleck, G. M. Muller, M. F. Ashby, and J. W. Hutchinson, "Strain Gradient Plasticity – Theory and Experiment," *Acta Metall. Mater.*, **42** [2] 475–87 (1994).
[55]J. S. Stolken and A. G. Evans, "A microbend Test Method for Measuring the Plasticity Length Scale," *Acta Mater.*, **46** [14] 5109–15 (1998).
[56]N. J. Petch, "The Cleavage Strength of Polycrystals," *J. Iron Steel I.*, **174** [1] 25–8 (1953).
[57]D. J. Lloyd, "Particle Reinforced Aluminum and Magnesium Matrix Composites," *Int. Mater. Rev*, **39**, 1–23 (1994).
[58]N. A. Fleck and J. W. Hutchinson, "Strain Gradient Plasticity," *Adv. Appl. Mech.*, **33**, 295–361 (1997).
[59]N. A. Fleck and J. W. Hutchinson, "A Reformulation of Strain Gradient Plasticity," *J. Mech. Phys. Solids*, **49** [10] 2245–71 (2001).
[60]H. Gao, Y. Huang, W. D. Nix, and J. W. Hutchinson, "Mechanism-Based Strain Gradient Plasticity – I. Theory," *J. Mech. Phys. Solids*, **47** [6] 1239–63 (1999).
[61]Y. Huang, H. Gao, W. D. Nix, and J. W. Hutchinson, "Mechanism-Based Strain Gradient Plasticity – II. Analysis," *J. Mech. Phys. Solids*, **48** [1] 99–128 (2000).
[62]W. D. Nix and H. J. Gao, "Indentation Size Effects in Crystalline Materials: A Law for Strain Gradient Plasticity," *J. Mech. Phys. Solids*, **46** [3] 411–25 (1998).
[63]A. G. Evans and J. W. Hutchinson, "A Critical Assessment of Theories of Strain Gradient Plasticity," *Acta Mater.*, **57** [5] 1675–88 (2009).
[64]M. F. Ashby, "Deformation of Plastically Non-Homogeneous Materials," *Philos. Mag.*, **21** [170] 399 (1970).
[65]D. M. Dimiduk, M. D. Uchic, and T. A. Parthasarathy, "Size-Affected Single-Slip Behavior of Pure Nickel Microcrystals," *Acta Mater.*, **53**, 4065–77 (2005).
[66]Z. W. Shan, R. Mishra, S. A. Syed, O. L. Warren, and A. M. Minor, "Mechanical Annealing and Source-limited Deformation in Submicron-diameter Ni Crystals," *Nat. Mater.*, **7** [116] 115–9 (2008).
[67]M. D. Uchic, D. M. Dimiduk, J. N. Florando, and W. D. Nix, "Sample Dimensions Influence Strength and Crystal Plasticity," *Science*, **305** [5686] 986–9 (2004).
[68]J. R. Greer, W. C. Oliver, and W. D. Nix, "Size Dependence of Mechanical Properties of Gold at the Micron Scale in the Absence of Strain Gradients," *Acta Mater.*, **53**, 1821–30 (2005).
[69]J. R. Greer and W. D. Nix, "Nanoscale Gold Pillars Strengthened through Dislocation Starvation," *Phys. Rev. B*, **73**, 245410–6 (2006).
[70]C. A. Volkert and E. T. Lilleodden, "Size Effects in the Deformation of Sub-Micron Au Columns," *Philos. Mag.*, **86**, 5567–79 (2006).
[71]A. Budiman, S. Han, J. R. Greer, N. Tamura, J. Patel, and W. D. Nix, "A Search for Evidence of Strain Gradient Hardening in Au Submicron Pillars Under Uniaxial Compression Using Synchrotron X-ray Microdiffraction," *Acta Mater.*, **56** [3] 602–8 (2007).
[72]D. Kiener, C. Motz, M. Rester, M. Jenko, and G. Dehm, "FIB Damage of Cu and Possible Consequences for Miniaturized Mechanical Tests," *Mater. Sci. Eng. A*, **459** [1–2] 262–72 (2006).
[73]G. Dehm, "Miniaturized Single-Crystalline fcc Metals Deformed in Tension: New Insights in Size-Dependent Plasticity," *Prog. Mater. Sci.*, **54** [6] 664–88 (2009).
[74]D. Kiener, C. Motz, T. Schoberl, M. Jenko, and G. Dehm, "Determination of Mechanical Properties of Copper at the Micron Scale," *Adv. Eng. Mater.*, **8** 1119–25 (2006).
[75]D. Kiener, W. Grosinger, G. Dehm, and R. Pippan, "A Further Step Towards an Understanding of Size-Dependent Crystal Plasticity: In Situ Tension Experiments of Miniaturized Single-Crystal Copper Samples," *Acta Mater.*, **56**, 580–92 (2008).
[76]D. Kiener, W. Grosinger, and G. Dehm, "On the Importance of Sample Compliance in Uniaxial Microtesting," *Scr. Mater.*, **60** [3] 148–51 (2009).
[77]D. Kiener, C. Motz, and G. Dehm, "Micro-Compression Testing: A Critical Discussion of Experimental Constraints," *Mater. Sci. Eng. A*, **505**, 79–87 (2009).
[78]R. Maass, S. Van Petegem, D. Grolimund, H. Van Swygenhoven, D. Kiener, and G. Dehm, "Crystal Rotation in Cu Single Crystal Micropillars:

In Situ Laue and Electron Backscatter Diffraction," *Appl. Phys. Lett*., 017905 (2008).
[79]A. T. Jennings and J. R. Greer, "Tensile Deformation of Electroplated Copper Nanopillars," *Phil. Mag. A*., **91** [7–9] 1108–20 (2010).
[80]A. T. Jennings, M. J. Burek, and J. R. Greer, "Size Effects in Single Crystalline cu Nano-Pillars Fabricated Without the Use of Fib," *Phys. Rev. Lett*., **104**, 135503 (2010).
[81]K. S. Ng and A. H. W. Ngan, "Breakdown of Schmid's Law in Micropillars," *Scr. Mater*., **59** [7] 796–9 (2008).
[82]K. S. Ng and A. H. W. Ngan, "Effects of Trapping Dislocations Within Small Crystals on Their Deformation Behavior," *Acta Mater*., **57**, 4902–10 (2009).
[83]H. Bei, E. P. George, and G. M. Pharr, "Small-Scale Mechanical Behavior of Intermetallics and Their Composites," *Mater. Sci. Eng. A*, **483–484**, 218–22 (2008).
[84]H. Bei, S. Shim, G. M. Pharr, and E. P. George, "Effects of Pre-Strain on the Compressive Stress–Strain Response of Mo-Alloy Single-Crystal Micropillars," *Acta Mater*., **56** [17] 4762–70 (2008).
[85]H. Bei and S. Shim, "Effects of Focused Ion Beam Milling on the Mechanical Behavior of a Molybdenum-Alloy Single Crystal," *Appl. Phys. Lett*., **91** [11] 11915 (2007).
[86]J.-Y. Kim, D. Jang, and J. R. Greer, "Insights into Deformation Behavior and Microstructure Evolution in Nb Single Crystalline Nano-Pillars Under Uniaxial Tension and Compression," *Scr. Mater*., **61** [3] 300–3 (2009).
[87]J. Y. Kim and J. R. Greer, "Tensile and Compressive Behavior of Gold and Molybdenum Single Crystals at the Nano-Scale," *Acta Mater*., **57** [17] 5245–53 (2009).
[88]J. Y. Kim, D. C. Jong, and J. R. Greer, "Tensile and Compressive Behavior of Tungsten, Molybdenum, Tantalum and Niobium at the Nanoscale," *Acta Mater*., **58** [7] 2355–63 (2010).
[89]A. S. Schneider, D. Kaufmann, B. G. Clark, C. P. Frick, P. A. Gruber, R. Monig, O. Kraft, and E. Arzt, "Correlation Between Critical Temperature and Strength of Small-Scale bcc Pillars," *Phys. Rev. Lett*., **103**, 105501 (2009).
[90]E. Lilleodden, "Microcompression Study of Mg (0001) Single Crystal," *Scr. Mater*., **62** [8] 532–5 (2010).
[91]C. M. Byer, B. Li, B. Cao, and K. T. Ramesh, "Microcompression of Single-Crystal Magnesium," *Scr. Mater*., **62** [8] 536–9 (2010).
[92]Q. Yu, Z.-W. Shan, J. Li, X. Huang, L. Xiao, J. Sun, and E. Ma, "Strong Crystal Size Effect on Deformation Twinning," *Nature*, **463**, 335–8 (2010).
[93]G. Lee, J.-Y. Kim, A. S. Budiman, N. Tamura, M. Kunz, K. Chen, M. J. Burek, J. R. Greer, and T. Y. Tsui, "Fabrication, Structure, and Mechanical Properties of Indium Nanopillars," *Acta Mater*., **58** [4] 1361–8 (2010).
[94]E. A. Withey, A. M. Minor, Jr, D. C. Morris, J. W. Morris, and S. Kuramot , "The Deformation of Gum Metal Through In Situ Compression of Nanopillars," *Acta Mater*., **58** [7] 2652–65 (2010).
[95]E. A. Withey, J. Ye, A. M. Minor, S. Kuramoto, D. C. Chrzan, and J. W. Morris Jr, "Nanomechanical Testing of Gum Metal," *Exp. Mech*., **50** 37–45 (2010).
[96]A. Rinaldi, P. Peralta, C. Friesen, and K. Sieradzki, "Sample-Size Effects in the Yield Behavior of Nanocrystalline Nickel," *Acta Mater*., **56** 511–7 (2008).
[97]D. Dang and J. R. Greer, "Size-Induced Weakening and Grain Boundary-Assisted Deformation in 60nm Grained Ni Nanopillars," *Scripta Mater*., **64**, 77–80 (2011).
[98]B. G. Clark, D. S. Gianola, O. Kraft, and C. P. Frick, "Size Independent Shape Memory Behavior of Nickel-Titanium," *Adv. Eng. Mater*., **12** [8] 805–15 (2010).
[99]C. P. Frick, S. Orso, and E. Arzt, "Loss of Pseudoelasticity in Nickel-Titanium Submicron Compression Pillars," *Acta Mater*., **55**, 3845–55 (2007).
[100]C. P. Frick, B. G. Clark, S. Orso, A. S. Schneider, and E. Arzt, "Size Effect on Strength an Strain Hardening of Small-Scale (111), Nickel Compression Pillars," *Mater. Sci. Eng. A*, **489** [1–2] 319–29 (2008).
[101]C. P. Frick, B. G. Clark, S. Orso, P. Sonnweber-Ribic, and E. Arzt, "Orientation-Independent Pseudoelasticity in Small-Scale NiTi Compression Pillars," *Scr. Mater*., **59**, 7–10 (2008).
[102]C. P. Frick, B. G. Clark, A. S. Schneider, R. Maaß, S. Van Petegem, and H. Van Swygenhoven, "On the Plasticity of Small-Scale Nickel-Titanium Shape Memory Alloys," *Scr. Mater*., **62**, 492–5 (2010).
[103]J. M. San Juan, M. L. Nó, and C. A. Schuh, "Nanoscale Shape-Memory Alloys for Ultrahigh Mechanical Damping," *Nat. Nanotechnol*., **4**, 415–9 (2009).
[104]J. M. San Juan, M. L. Nó, and C. A. Schuh, "Superelasticity and Shape Memory in Micro- and Nanometer-Scale Pillars," *Adv. Mater*., **20**, 272–8 (2008).
[105]D. Jang and J. R. Greer, "Transition From a Strong-Yet-Brittle to a Stronger-and-Ductile State by Size Reduction of Metallic Glasses," *Nat. Mater*., **9**, 215–9 (2010).
[106]C. A. Volkert, A. Donohue, and F. Spaepen, "Effect of Sample Size on Deformation in Amorphous Metals," *J. Appl. Phys*., **103** [8] 083539 (2008).
[107]C. Q. Chen, Y. T. Pei, and J. T. M. De Hosson, "Strength of Submicrometer Diameter Pillars of Metallic Glasses Investigated with in Situ Transmission Electron Microscopy," *Philos. Mag. Lett*., **89** [10] 633–40 (2009).
[108]M. D. Uchic, P. A. Shade, and D. M. Dimiduk, "Plasticity of Micrometer-Scale Single Crystals in Compression," *Annu. Rev. Mater. Res*., **39** [1] 361–86 (2009).
[109]R. Dou and B. Derby, "A Universal Scaling Law for the Strength of Metal Micropillars and Nanowires," *Scr. Mater*., **61** [5] 524–7 (2009).
[110]C. V. Thompson, "The Yield Stress of Polycrystalline Thin Films," *J. Mater. Res*., **8**, 237 (1993).
[111]B. von Blanckenhagen, P. Gumbsch, and E. Arzt, "Dislocation Sources and the Flow Stress of Polycrystalline Thin Metal Films," *Philos. Mag. Lett*., **83** [1] 1–8 (2003).
[112]M. S. De Guzman, G. Neubauer, P. Flinn, and W. D. Nix, "The Role of Indentation Depth on the Measured Hardness of Materials," *Mater. Res. Soc. Symp. Proc*., **308** 613 (1993).
[113]J. R. Greer, W. C. Oliver, and W. D. Nix, "Size Dependence of Mechanical Properties of Gold at the Micron Scale in the Absence of Strain Gradients," *Acta Mater*., **53** [6] 1821–30 (2005).
[114]K. S. Ng and A. H. W. Ngan, "Stochastic Nature of Plasticity of Aluminum Micro-Pillars," *Acta Mater*., **56** [8] 1712–20 (2008).
[115]S. I. Rao, D. M. Dimiduk, T. A. Parthasarathy, M. D. Uchic, M. Tang, and C. Woodward, "Athermal Mechanisms of Size-Dependent Crystal Flow Gleaned From Three-Dimensional Discrete Dislocation Simulations," *Acta Mater*., **56** [13] 3245–59 (2008).
[116]D. M. Norfleet, D. M. Dimiduk, S. J. Polasik, M. D. Uchic, and M. J. Mills, "Dislocation Structures and Their Relationship to Strength in Deformed Nickel Microcrystals," *Acta Mater*., **56** [13] 2988–3001 (2008).
[117]T. A. Parthasarathy, S. I. Rao, D. M. Dimiduk, M. D. Uchic, and D. R. Trinkle, "Contribution to size effect of yield strength from the stochastics of dislocation source lengths in finite samples," *Scr. Mater*., **56** [4] 313–6 (2007).
[118]S. I. Rao, D. M. Dimiduk, M. Tang, T. A. Parthasarathy, M. D. Uchic, and C. Woodward, "Estimating the Strength of Single-Ended Dislocation Sources in Micron-Sized Single Crystals," *Philos. Mag. A*, **87** [30], 4777–94 (2007).
[119]D. M. Dimiduk, C. Woodward, R. LeSar, and M. D. Uchic, "Scale-Free Intermittent Flow in Crystal Plasticity," *Science*, **312**, 1188–90 (2006).
[120]O. Kraft, P. A. Gruber, R. Monig, and D. Weygand, "Plasticity in Confined Dimensions," *Annu. Rev. Mater. Res*., **40**, 293–317 (2010).
[121]A. T. Jennings, M. J. Burek, and J. R. Greer, "Size Effects in Single Crystalline cu Nano-Pillars Fabricated Without the Use of Fib," *Phys. Rev. Lett*., **104**, 135503 (2010).
[122]S. Lee, S. Han, and W. D. Nix, "Uniaxial Compression of fcc Au Nanopillars on an MgO Substrate: The Effects of Prestraining and Annealing," *Acta Mater*., **57** [15] 4404–15 (2009).
[123]S. Shim, H. Bei, M. K. Miller, G. M. Pharr, and E. P. George, "Effects of Focused Ion Beam Milling on the Compressive Behavior of Directionally Solidified Micropillars and the Nanoindentation Response of an Electropolished Surface," *Acta Mater*., **57**, 503–10 (2009).
[124]J. A. El-Awady, C. Woodward, D. M. Dimiduk, and N. M. Ghoniem, "Effects of Focused Ion Beam Induced Damage on the Plasticity of Micropillars," *Phys. Rev. B*, **80**, 104104 (2009).
[125]R. Ikeda, H. Ogi, T. Ogawa, and M. Takemoto, "Mechanical Properties of CVD Synthesized Polycrystalline Diamond," *Ind. Diamond Quat*., **69**, 35–8 (2009).
[126]N. A. Fleck, V. Deshpande, and M. F. Ashby, "Micro-Architected Materials: Past, Present and Future," *Proc. Royal Soc. A*, **466**, 2495–516 (2010).
[127]D. J. Bell, T. J. Lu, N. A. Fleck, and S. M. Spearing, "MEMS Actuators and Sensors: Observations on Their Performance and Selection for Purpose," *J. Micromech. Microeng*., **15** [7] S153–64 (2005).
[128]M. A. Haque and T. Saif, "Mechanical Testing at the Micro/Nano Scale." in *Springer Handbook of Experimental Solid Mechanics*. Edited by W. N. Sharpe. Springer, New York, 2008.
[129]A. Torrents, K. Azgin, S. W. Godfrey, E. S. Topalli, T. Akin, and L. Valdevit, "MEMS Resonant Load Cells for Micro-Mechanical Test Frames: Feasibility Study and Optimal Design," *J. Micromech. Microeng*., **20** 125004 (17pp) (2010).
[130]F. Giessibl, "Advances in Atomic Force Microscopy," *Rev. Mod. Phys*., **75** [3] 949–83 (2003).
[131]P. Hinterdorfer and Y. Dufrene, "Detection and Localization of Single Molecular Recognition Events Using Atomic Force Microscopy," *Nat. Methods*, **3** [5] 347–55 (2006).
[132]G. Schitter and M. J. Rost, "Scanning Probe Microscopy at Video-Rate," *Mater. Today*, **11**, 40–8 (2008).
[133]M. D. Kriese, W. W. Gerberich, and N. R. Moody, "Quantitative Adhesion Measures of Multilayer Films: Part I. Indentation Mechanics," *J. Mater. Res*., **14** [7] 3007–18 (1999).
[134]M. D. Kriese, W. W. Gerberich, and N. R. Moody, "Quantitative Adhesion Measures of Multilayer Films: Part II. Indentation of W/Cu, W/W, Cr/W," *J. Mater. Res*., **14** [7] 3019–26 (1999).
[135]E. T. Lilleodden, W. Bonin, J. Nelson, J. T. Wyrobek, and W. W. Gerberich, "In-Situ Imaging of MU-N Load Indents into GAAS," *J. Mater. Res*., **10** [9] 2162–5 (1995).
[136]W. D. Nix, "Elastic and Plastic Properties of Thin Films on Substrates: Nanoindentation Techniques," *Mat. Sci. Eng. A - Struct*., **234**, 37–44 (1997).
[137]W. C. Oliver and G. M. Pharr, "An Improved Technique for Determining Hardness and Elastic Modulus Using Load and Displacement Sensing Indentation Experiments," *J. Mater. Res*., **7** [6] 1564–83 (1992).
[138]W. C. Oliver and G. M. Pharr, "Measurement of Hardness and Elastic Modulus by Instrumented Indentation: Advances in Understanding and Refinements to Methodology," *J. Mater. Res*., **19** [1] 3–20 (2004).
[139]J. R. Greer, J.-Y. Kim, and M. J. Burek, "The In-Situ Mechanical Testing of Nanoscale Single-Crystalline Nanopillars," *J. Mater*., **61** [12] 19–25 (2009).
[140]J.-Y. Kim and J. R. Greer, "Tensile and Compressive Behavior of Gold and Molybdenum Single Crystals at the Nano-Scale," *Acta Mater*., **57**, 5245–53 (2009).
[141]Z. Y. Xue and J. W. Hutchinson, "Constitutive Model for Quasi-Static Deformation of Metallic Sandwich Cores," *Int. J. Numer. Meth. Eng*., **61** [13] 2205–38 (2004).

[142]J. E. Angelo, N. R. Moody, and M. I. Baskes, "Trapping of Hydrogen to Lattice-Defects in Nickel," *Modelling Simul. Mater. Sci. Eng.*, **3** [3] 289–307 (1995).
[143]M. I. Baskes, "Modified Embedded-Atom Potentials for Cubic Materials," *Phys. Rev. B*, **46** [5] 2727–42 (1992).
[144]W. Xiao, M. I. Baskes, and K. Cho, "MEAM Study of Carbon Atom Interaction With Ni Nano Particle," *Surf. Sci.*, **603** [13] 1985–98 (2009).
[145]Y. Jiang, Y. G. Wei, J. R. Smith, J. W. Hutchinson, and A. G. Evans, "First Principles Based Predictions of the Toughness of a Metal/Oxide Interface," *Int. J. Mater. Res.*, **101** [1] 8–15 (2010).
[146]V. S. Deshpande, A. Needleman, and E. Van der Giessen, "Plasticity Size Effects in Tension and Compression of Single Crystals," *J. Mech. Phys. Solids*, **53** [12] 2661–91 (2005).
[147]H. Tang, K. W. Schwarz, and H. D. Espinosa, "Dislocation-Source Shutdown and the Plastic Behavior of Single-Crystal Micropillars," *Phys. Rev. Lett.*, **100**, 185503 (2008).
[148]E. Van der Giessen and A. Needleman, "Discrete Dislocation Plasticity – A Simple Planar Model," *Modelling Simul. Mater. Sci. Eng.*, **3** [5] 689–735 (1995).
[149]M. D. Uchic, P. A. Shade, and D. M. Dimiduk, "Plasticity of Micrometer-Scale Single Crystals in Compression," *Annu. Rev. Mater. Res.*, **39**, 361–86 (2009).
[150]J. Wang, A. G. Evans, K. Dharmasena, and H. N. G. Wadley, "On the Performance of Truss Panels With Kagome Cores," *Int. J. Solids Struct.*, **40** [25] 6981–8 (2003).
[151]M. P. Bendsoe and O. Sigmund, "*Topology Optimization*," pp. 370. Springer, Berlin, Germany, (2002).
[152]P. W. Christensen and A. Klabring, "*An Introduction to Structural Optimization*," pp. 214. Springer, Berlin, Germany, (2008).
[153]O. Sigmund and S. Torquato, "Design of Materials With Extreme Thermal Expansion Using a Three-Phase Topology Optimization Method," *J. Mech. Phys. Solids*, **45** [6] 1037–67 (1997).
[154]O. Sigmund and S. Torquato, "Design of Smart Composite Materials Using Topology Optimization," *Smart Mater. Struct.*, **8** [3] 365–79 (1999).
[155]S. Hyun and S. Torquato, "Optimal and Manufacturable Two-Dimensional, Kagome-Like Cellular Solids," *J. Mater. Res.*, **17** [1] 137–44 (2002).
[156]A. J. Jacobsen, W. Barvosa-Carter, and S. Nutt, "Micro-Scale Truss Structures With Three-Fold And Six-Fold Symmetry Formed From Self-Propagating Polymer Waveguides," *Acta Mater.*, **56** [11] 2540–8 (2008).
[157]A. J. Jacobsen, S. Mahoney, W. B. Carter, and S. Nutt, "Vitreous Carbon Micro-Lattice Structures," *Carbon*, **49** [3] 1025–32 (2011).
[158]J. R. Greer and J. T. M. De Hosson, "Plasticity in Small-Sized Metallic Systems: Intrinsic Versus Extrinsic Size Effects," *Prog. Mater. Sci.*, **56**, 654–724 (2011).
[159]J.-Y. Kim and J. R. Greer, "Size-Dependent Mechanical Properties of Mo Nanopillars," *Appl. Phys. Lett.*, **93**, 101916 (2008).
[160]A. J. Jacobsen, W. Barvosa-Carter, and S. Nutt, "Compression Behavior of Micro-Scale Truss Structures Formed From Self-Propagating Polymer Waveguides," *Acta Mater.*, **55** [20] 6724–33 (2007).
[161]K. Azgin, C. Ro, A. Torrents, T. Akin, and L. Valdevit, "A Resonant Tuning Fork Sensor with Unprecedented Combination of Resolution and Range." in *IEEE MEMS Conference*, Paper # 0700. Cancun, Mexico, 2011.